Phase diagrams of ferromagnet-superconductor multilayers with misaligned exchange fields

Tomas Löfwander, Thierry Champel, and Matthias Eschrig
Institut für Theoretische Festkörperphysik, Universität Karlsruhe, D-76128 Karlsruhe, Germany
(Received 7 May 2006; revised manuscript received 16 November 2006; published 10 January 2007)

We study the influence of misalignment of the ferromagnetic exchange field on the equilibrium properties of hybrid structures, composed of superconducting (S) and ferromagnetic (F) parts. In particular, we study numerically the superconducting critical temperature T_c in F-S-F trilayers and in F-S-F-S-F Josephson junctions as a function of the misalignment angle θ of the ferromagnetic magnetization. We discuss the corresponding phase diagrams for these hybrid structures. For the Josephson junctions, a transition between the zero-phase and the π-phase ground states as a function of θ takes place under certain conditions. Within the quasiclassical Green's function technique in the diffusive limit, we introduce a fast and effective method for calculating T_c in such multilayer structures.

DOI: 10.1103/PhysRevB.75.014512 PACS number(s): 74.45.+c, 74.62.−c, 74.78.Fk, 74.25.Dw

I. INTRODUCTION

The interest in superconductor-ferromagnet (S-F) hybrid structures has considerably increased in the last decade due to their relevance for the development of nanometer scale electronic devices. The understanding of the superconducting proximity effect in S-F devices is of vital importance for such a goal. Consequently, experimental and theoretical studies have focused on the influence that proximity induced spin-triplet pairing amplitudes in S-F hybrid structures have on superconducting properties of the entire structure. Among those are, for example, changes of the superconducting transition temperature T_c of the device, or the switching between 0 junctions and π junctions as ground states in S-F-S Josephson devices as a function of some control parameter.

The superconducting critical temperature T_c in diffusive hybrid S-F structures has been studied both theoretically[1–11] and experimentally[12–23] in several recent publications. It has been shown[1,2] that T_c has a nonmonotonic dependence on the thickness d_f of the ferromagnetic layers that provide information about the strength of the ferromagnetic exchange field and about the transparencies of the S-F interfaces. Approximate analytic formulas for T_c have been derived for several limiting cases,[24] e.g., for thin or thick film thicknesses or for low or high interface resistances. Recently, Fominov *et al.* developed a numerical method to compute T_c for diffusive S-F bilayers[8] and symmetric F-S-F trilayers[10] for arbitrary model parameters such as layer thicknesses and interface resistances. Such an approach is valuable when theory and experiments are compared in detail with the aim to extract parameters as, e.g., the ferromagnetic exchange field or the boundary transparencies.

The possibility[1,24,25] of a π state (characterized by a stable phase difference of π between the superconducting order parameters) is now well established experimentally in S-F hybrid structures involving several superconducting layers. Transitions between the 0 and π states have been revealed in S-F-S junctions by the oscillations of the critical current when varying the temperature[26–28] or the ferromagnetic thickness.[29–31] The transitions from the 0 to π state may also be revealed[2] by the presence of cusps in the dependence of T_c on d_f. Because the cusps may be confounded with the oscillations of $T_c(d_f)$ themselves, such a feature in the dependence of T_c has been identified experimentally only recently.[18,32]

The presence of several ferromagnetic layers introduces a new degree of freedom, the relative orientation angle, θ, between the magnetizations. The influence of the orientation on T_c was first studied theoretically in F-S-F trilayers in Refs. 5 and 6 (these authors only considered parallel or antiparallel orientations). Calculations for arbitrary orientations were performed in Ref. 10. A dependence of the critical current oscillations on the magnetization orientation has also been established theoretically in S-F-F′-S junctions[33–36] and multilayered S-F junctions.[37] In Refs. 34 and 37 a switch between the 0 and π states has been found from calculations of the Josephson critical current by changing the mutual orientation between the moments. The dependence of T_c on the moment orientation (parallel or antiparallel) of trilayers has been studied experimentally in Refs. 16 and 20–22. A dependence on the domain state of the ferromagnet in S-F bilayer and multilayers was found in Refs. 17 and 23.

Motivated by the recent experimental studies, we have developed a fast and effective method that is particularly suited for the numerical calculation of T_c in diffusive hybrid structures. An important part of this paper is to present details of this method and discuss the calculations leading to some of the results presented in Ref. 32. Our method can be considered as a development of the method of Fominov *et al.*, who in Refs. 8 and 10 have presented calculations of T_c of S-F bilayers and symmetric F-S-F trilayers with noncollinear magnetizations. We extend the calculations to the more general case of asymmetric trilayers in connection with the geometry considered typically in experiments. Within our model, we also treat symmetric pentalayers, including the possibility of a phase difference π between the two superconductors. This structure was recently studied experimentally in Ref. 32. From our T_c calculations, we predict a switching between 0 junctionss and π junctions by the orientation of the ferromagnetic exchange fields in pentalayers consisting of a central Josephson junction, two superconductors separated by a ferromagnet, sandwiched between two outer ferromagnets with exchange fields rotated relative to the central ferromagnetic layer. This kind of structure could

be realized, e.g., by fixing the moments of the outer layers, while rotating the moment of the central layer with an external magnetic field.

The outline of the paper is as follows. In Sec. II we present the model of the F-S-F trilayer and the F-S-F-S-F pentalayer structures and outline the method that we use to compute the order parameter profile and T_c of the structures. In Secs. III and IV we present the results for the trilayer and pentalayer, respectively. In Sec. V we discuss some details of our numerical method. We summarize our work in Sec. VI. Some of the technical details have been collected in the Appendices.

In this paper we use units for which $\hbar=1=k_B$.

II. MODEL AND METHOD

We shall restrict our considerations to diffusive hybrid structures and to temperatures T near the critical temperature T_c. We employ a Green's function method in the quasiclassical approximation. The central quantity in this framework is the 2×2 spin-matrix anomalous Green's function f, describing superconducting correlations in the structure. The spin degree of freedom has to be kept due to the fact that the ferromagnets in proximity with the superconductors break spin rotation invariance. Thus, both spin singlet and spin triplet proximity pair amplitudes are present in the ferromagnet. We use a notation where the spin structure is described as $f=(f_s+\boldsymbol{\sigma}\cdot\mathbf{f}_t)i\sigma_y$, where $\boldsymbol{\sigma}=(\sigma_x,\sigma_y,\sigma_z)$ are the three Pauli matrices. The pair amplitudes are the spin singlet component f_s and the three spin triplet components described by the vector $\mathbf{f}_t$. The ferromagnetic regions are characterized by an exchange field with a fixed direction. In the case of rapid changes on the scale of the coherence length of the direction of the exchange field,[38–40] or spin-active interface scattering,[41] long-range equal-spin triplet correlations are also induced. We refer to our recent papers[41–44] and a recent review[45] and references therein for a deeper discussion of the origin of these correlations.

The quasiclassical approximation is appropriate for systems with a set of well separated energy scales: a low-energy scale and a high-energy scale. The high-energy scale is set by the Fermi energy ϵ_f. The superconducting gap Δ is in the low-energy range. In a system with a nonzero exchange field J, the quasiclassical approximation is applicable only for the two limiting cases for which J is in either the low-energy range or in the high-energy range. The first case, $J\ll\epsilon_f$, is the appropriate case for dilute ferromagnetic metals or ferromagnets with a weak exchange splitting. In the second case J is comparable with the Fermi energy, and the Fermi surface is split into well separated branches that are classified according to their spin. This is the appropriate case for ferromagnets with strong exchange splitting. A special case that has been treated in such a way is the case of a half-metal.[41] Note that the crossover of J from the low- to the high-energy range cannot be described by a quasiclassical approach.

For structures containing impurity disorder yet another energy scale enters the problem: $1/\tau$, where τ is the elastic impurity scattering time. The associated length scale is given by the mean free path, $\ell=v_f\tau$. In order for the quasiclassical approximation to be applicable, the inequality $1/\tau\ll\epsilon_f$ (or equivalently, $\lambda_f\ll\ell$, where λ_f is the Fermi wavelength) must hold. We concentrate in this paper on the diffusive limit within quasiclassical theory, which is applicable when $\Delta\ll 1/\tau\ll\epsilon_f$.

For diffusive structures the Green's function is isotropic to lowest order in $\tau\Delta$. Furthermore, for temperatures near the critical temperature the superconducting gap is small $\Delta\ll T_c$ and the usual Green's function is approximately equal to the normal-state Green's function $g\approx -i\pi\,\mathrm{sgn}(\varepsilon_n)$, while the anomalous Green's function f is small, of the order of Δ. The relevant starting point in this case is Usadel's diffusion equation[46] linearized for small Δ. We assume for simplicity that the spatial dependence in the structure is only along the interface normal, taken to be along the x axis, see Figs. 1 and 8. Then, the linearized Usadel equations have the form[43]

$$(D\partial_{xx}^2-2|\varepsilon_n|)f_s=-2\pi\Delta+2i\,\mathrm{sgn}(\varepsilon_n)\mathbf{J}\cdot\mathbf{f}_t, \tag{1}$$

$$(D\partial_{xx}^2-2|\varepsilon_n|)\mathbf{f}_t=2i\,\mathrm{sgn}(\varepsilon_n)\mathbf{J}f_s, \tag{2}$$

where $\mathrm{sgn}(\varepsilon_n)$ is the sign of the Matsubara frequency $\varepsilon_n=\pi T(2n+1)$ (n=integer), and we have used the short-hand notation $f=f(\varepsilon_n,x)$. We assume that the exchange field $\mathbf{J}=\mathbf{J}(x)$ is nonzero in the ferromagnetic regions, while $\Delta=\Delta(x)$ is nonzero in the superconducting regions. Each layer in the structure can have a different diffusion constant D.

Note that the diffusive approximation puts a constraint on the size of the exchange fields we can consider, namely $J\tau\ll 1$. This inequality is equivalent to $\ell\ll v_f/J$, where v_f/J is the clean limit magnetic length. There exists, however, a parameter regime $v_f/J\lesssim\ell$ but still $\ell\ll\xi_0$, where $\xi_0=v_f/\Delta$ is the clean limit superconducting coherence length. In this case the quasiclassical Eilenberger equations have to be solved, see Refs. 36, 47, and 48. In Ref. 48 it was argued that for $3d$ transition metals $s-d$ scattering is important and leads to different mean free paths for up- and down-spin bands. Such effects are beyond the scope of the present paper.

The above diffusion equation is supplemented with boundary conditions at each interface and at the outer surfaces of the structure. The boundary condition connecting the Green's function on the superconductor side of the interface (denoted x_s) with the Green's function on the ferromagnet side of the interface (denoted x_f) is of the form first derived by Kupriyanov and Lukichev:[49]

$$\gamma\xi_f f'(x_f)=\xi_s f'(x_s), \tag{3}$$

$$\gamma_b\xi_f f'(x_f)=\pm[f(x_s)-f(x_f)], \tag{4}$$

where $\xi_s=\sqrt{D_s/2\pi T_{c0}}$ and $\xi_f=\sqrt{D_f/2\pi T_{c0}}$ are coherence lengths in the S and F sides. The parameters γ and γ_b characterize the conductivity mismatch between the two sides and the boundary resistance, respectively. The sign in Eq. (4) is positive (negative) for a F/S (S/F) interface, for which the superconductor occupies the space to the right (left) of the barrier. Note that we use the prime as a short-hand notation for spatial derivatives at a certain point in space, e.g., $f'(x_s)=\partial_x f(x)|_{x=x_s}$. At the outer surfaces of the structure, we

require that the current through the boundary must vanish, i.e., $\partial_x f=0$.

Since the exchange field and the superconducting order parameter are spatially separated, we see that in the superconducting region Eqs. (1) and (2) are decoupled. The triplet part (2) can be solved analytically, while the singlet part (1) has a source term containing the order parameter that satisfies the self-consistency equation

$$\Delta(x)\ln\frac{T}{T_{c0}}=T\sum_{\varepsilon_n}\left(f_s(\varepsilon_n,x)-\frac{\pi\Delta(x)}{|\varepsilon_n|}\right). \tag{5}$$

In the ferromagnetic regions Eqs. (1) and (2) are coupled but the superconducting order parameter is absent and both equations can be solved analytically, which is described in detail in Appendices A and B for the trilayer and pentalayer cases. The presence of the ferromagnetic regions is in the process reduced to an effective boundary condition for the calculation of the singlet component in the superconducting region, which we confine to $0<x<d_s$ in the present discussion, as in Fig. 1. The boundary condition can in the general case be written in the form

$$\begin{pmatrix} f_s'(0) \\ f_s'(d_s) \end{pmatrix}=k_s\hat{W}\begin{pmatrix} f_s(0) \\ f_s(d_s) \end{pmatrix}, \tag{6}$$

where $k_s=\sqrt{2\varepsilon_n/D_s}$ and $\hat{W}$ is a 2×2 matrix. The nonlocality of the boundary condition (6), i.e., the coupling of the two interfaces at 0 and at d_s, is a result of the coupling of the singlet and triplet anomalous Green's functions f_s and $\mathbf{f}_t$ in the original boundary conditions Eqs. (3) and (4) and the coupling of the diffusion equations for the singlet and triplet components in the ferromagnet by the exchange field. The matrix $\hat{W}$ depends on the Matsubara frequency, the parameters of the adjacent layers (thicknesses, exchange fields, diffusion constants), and the interface parameters γ and γ_b. The expressions for the components of $\hat{W}$ are derived in Appendices A and B for the trilayer and pentalayer structures. The following method for calculating T_c is, however, applicable for any matrix $\hat{W}$, as long as the boundary condition for the singlet Green's function f_s is of the form (6).

Consider Eq. (1) in the superconducting region, i.e., for $0<x<d_s$ where $\mathbf{J}=0$. By linear superposition we have[8]

$$f_s(\varepsilon_n,x)=\pi\int_0^{d_s}G(\varepsilon_n,x,y)\Delta(y)dy, \tag{7}$$

where the function $G(\varepsilon_n,x,y)$ is the solution of the differential equation

$$\left(\frac{D_s}{2}\partial_{xx}^2-|\varepsilon_n|\right)G(\varepsilon_n,x,y)=-\delta(x-y), \tag{8}$$

subject to the boundary conditions (6) with $f_s(\varepsilon_n,x)$ replaced by $G(\varepsilon_n,x,y)$. The solution of Eq. (8) is presented in Appendix C. With the help of the function G, the gap equation can be written as

$$\frac{2\pi T\sum_{\varepsilon_n>0}\int_0^{d_s}G(\varepsilon_n,x,y)\Delta(y)dy}{\ln\frac{T}{T_{c0}}+2\pi T\sum_{\varepsilon_n>0}(\varepsilon_n)^{-1}}=\Delta(x), \tag{9}$$

where we used that the singlet Green's function $f_s(\varepsilon_n,x)$ [and therefore also $G(\varepsilon_n,x,y)$] is an even function of ε_n. We see that one way[8] of solving the problem at hand is to discretize the spatial coordinate ($x\to x_k$, $k=1,\ldots,N$) and find the critical temperature T_c as the highest temperature for which the eigenvalue of the $N\times N$ matrix on the left-hand side of Eq. (9) equals 1. The corresponding eigenvector gives the profile of the order parameter $\Delta(x_k)$.

There are several disadvantages of the method described above, all connected with the discretization of the spatial coordinate axis. In particular, it is cumbersome to reach acceptable numerical accuracy when T_c is computed. We shall discuss these problems in detail in Sec. V.

Because of these drawbacks, we develop a Fourier series method and thereby avoid the discretization of the spatial coordinate. The superconducting order parameter $\Delta(x)$ exists in the range $0<x<d_s$. We extend its domain of definition to the full real axis by adding an even-parity property and $2d_s$ periodicity. Then, $\Delta(x)$ can be expanded in a Fourier series

$$\Delta(x)=\sum_{p=0}^{\infty}\Delta_p\cos\left(\frac{p\pi x}{d_s}\right), \tag{10}$$

where the coefficients Δ_p are defined as

$$\Delta_p=\frac{2-\delta_{p0}}{d_s}\int_0^{d_s}\Delta(x)\cos\left(\frac{p\pi x}{d_s}\right)dx. \tag{11}$$

We show in Appendix D how to obtain an analytic expression for the singlet amplitude f_s in terms of the Fourier coefficients Δ_p. Consequently, the gap equation can be written in the space of Fourier coefficients as

$$\sum_{p=0}^{\infty}m_{lp}\Delta_p=0, \tag{12}$$

for integer $l\geq 0$, and where m_{lp} are given in Eqs. (D3) and (D4). We solve the problem at hand by introducing a cutoff p_c for the number of harmonics and find the critical temperature T_c as the highest temperature for which the eigenvalue of the $p_c\times p_c$ matrix on the left-hand side of Eq. (12) equals 0. The corresponding eigenvector gives the profile of the order parameter $\Delta(x)$ through the sum in Eq. (10).

In the following two sections we use this method to compute T_c for the S-F trilayer and pentalayer structures. In Sec. V we discuss the advantages of our method [Eq. (12)] and compare with the other method [Eq. (9)].

III. TRILAYER

Consider the trilayer structure shown in Fig. 1. We study in this section the superconducting transition temperature of such a trilayer. Our studies are motivated by the recent ex-

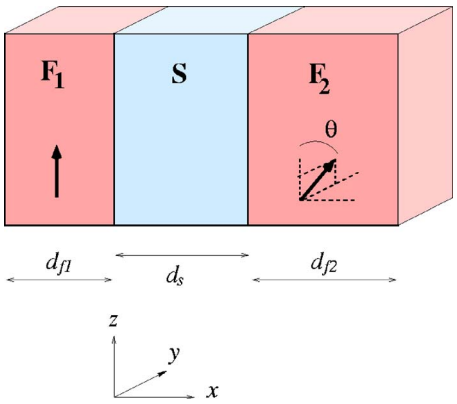

FIG. 1. (Color online) Geometry of the asymmetric F_1-S-F_2 structure. The moments $\mathbf{J}_1$ (in F_1) and $\mathbf{J}_2$ (in F_2) may have different amplitudes and point in different directions (the relative orientation angle is denoted θ).

periments on S-F layered structures,[12–16,18–22] including in particular the experiments in Ref. 32 on the critical temperature of asymmetric F_1-S-F_2 trilayers. The theory fits of T_c of the trilayers in Ref. 32 were obtained with the theory presented in the present paper.

In the left ferromagnetic layer (F_1), the exchange field is aligned with the z axis, while in F_2 it lies in the yz plane and forms an angle θ with respect to the z axis. The origin of the coordinate system is taken at the F_1/S interface. The two layers F_1 and F_2 are characterized by their thicknesses (d_{f1}, d_{f2}), exchange fields (J_1, J_2), and diffusion constants (D_{f1}, D_{f2}), while the superconducting layer is characterized by its thickness (d_s), pairing interaction strength (i.e., the bulk material superconducting critical temperature T_{c0}), and diffusion constant (D_s). The diffusion constants are converted into coherence lengths $\xi=\sqrt{D/2\pi T_{c0}}$ and we shall use the coherence length in the superconductor ξ_s as length scale in the problem. The F_1/S and S/F_2 interfaces are characterized by the conductivity mismatches (γ_1, γ_2) and interface resistances (γ_{b1}, γ_{b2}).

The Usadel equations (1) and (2) are solved as described in Appendix A to give the effective boundary condition matrix $\hat{W}$ for the trilayer. The matrix m_{lp} of Eq. (12) is then given in terms of the elements of $\hat{W}$ as shown in Appendix D.

TABLE I. Key to the symbols of the model parameters.

T_{c0}	Bulk critical temperature
T_c	Layer critical temperature
Δ	Order parameter
D	Diffusion constant
$\xi=\sqrt{\frac{D}{2\pi T_{c0}}}$	Coherence length
d	Layer thickness
J	Exchange field
θ	Exchange field misorientation angle
γ	Materials conductivity mismatch
γ_b	Boundary resistance parameter

A. Results

In Table I we present a key to the symbols of the model parameters. In Table II we present values of the model parameters used in Figs. 2–7. In Fig. 2 we present the influence of an exchange field on T_c for an asymmetric F_1-S-F_2 trilayer (with $d_{f1} \neq d_{f2}$). In the normal metal case (obtained by setting $J=0$), the critical temperature is monotonically suppressed as the layer thickness d_{f1} is increased. In the case of a ferromagnet, the exchange field induces an additional oscillatory behavior, closely connected to the spin mixing between up and down spins. As a result, T_c is suppressed in a nonmonotonic way. For a strong-enough exchange field, the oscillation is so strong that superconductivity is suppressed at a critical thickness but can reappear at a larger thickness. This kind of nonmonotonic dependence of T_c was thoroughly studied[4–6,8,10,11,24] for F-S bilayers and symmetric F-S-F trilayers.

We show the influence of having different thicknesses d_{f1} and d_{f2} of the two F layers in Fig. 3. Previously published results are contained in the figure: the cuts $d_{f1}=0$ (or $d_{f2}=0$) correspond to a F/S bilayer,[8] while the diagonal cut d_{f1}

TABLE II. Values of the model parameters used in Figs. 2–7. The meanings of the parameters are listed in Table I. The sign ~ indicates that the parameter is varied in the figure. The subscripts s, $f1$, and $f2$ refer to the superconductor, ferromagnet 1, and ferromagnet 2, respectively. Note that in all figures we have $\gamma_1=\gamma_2=\gamma$, $\gamma_{b1}=\gamma_{b2}=\gamma_b$, $J_1=J_2=J$, and finally $D_{f1}=D_{f2}=D_s$ which means $\xi_{f1}=\xi_{f2}=\xi_s$. The length unit is ξ_s and the energy unit is T_{c0}. γ and γ_b are dimensionless.

	Parameter values for the trilayer						
Figure no.	d_s	d_{f1}	d_{f2}	J	θ	γ	γ_b
2	2	~	0.5	~	0	0.3	0.7
3	2	~	~	20	0	0.3	0.7
4	2	~	0.5	20	0	0.3	~
5	~	0.2	0.5	20	0	~	~
6	2	~	0.5	20	~	0.3	0.7
7	2	0.1	0.5	20	0	0.3	~

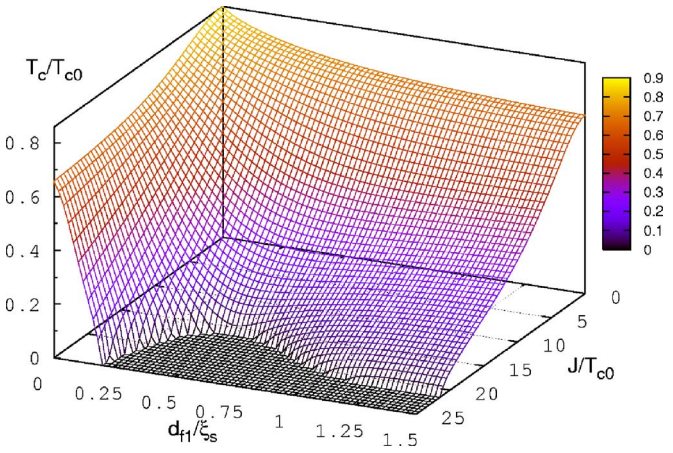

FIG. 2. (Color online) The critical temperature T_c of a trilayer for a variety of thicknesses d_{f1} and exchange fields J. The model parameters are given in Table II. Note that T_c/T_{c0} for $d_{f1}=0=J$ is suppressed to ≈ 0.86 because $d_{f2}=0.5\xi_s$.

$=d_{f2}$ corresponds to a symmetric trilayer F-S-F with aligned exchange fields.[10] For an asymmetric layer, one layer (e.g., F_2) can be used to suppress the initial T_c at $d_{f1}=0$ sufficiently that the following dependence $T_c(d_{f1})$ shows strong oscillatory behavior[32] including disappearing and reappearing superconductivity.

The exact point where superconductivity disappears and reappears depends on other parameters in addition to the strength of the exchange field and the ferromagnetic layer thicknesses. In particular, T_c is sensitive to the quality of the interfaces (here represented by the resistance parameter γ_b) and the conductivity mismatch γ between the ferromagnetic and superconducting materials. For example, we show in Fig. 4 how superconductivity is suppressed in trilayers with good contacts (small γ_b). We present in Fig. 5 phase diagrams showing the critical thickness d_s of the superconductor where $T_c \to 0$ as function of the conductivity mismatch for a few interface resistances. In this figure we clearly see that it is not possible to consider $d_s \ll \xi_s$, for which simplified theoretical calculations with a constant Δ throughout the structure can be made, and simultaneously consider good contacts $\gamma_b \to 0$, unless the conductivity mismatch is very small. It is therefore always important to keep in mind that T_c is suppressed to zero in quite a large parameter space, including small d_s and small γ_b for reasonable values of γ.

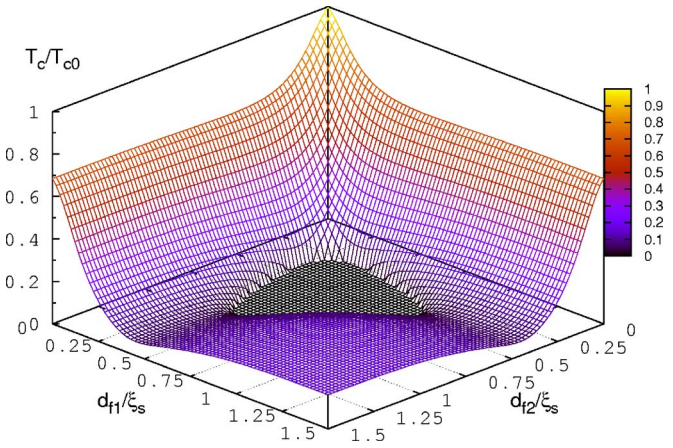

FIG. 3. (Color online) Critical temperature T_c of a trilayer versus the thicknesses of the ferromagnetic layers. The model parameters are given in Table II.

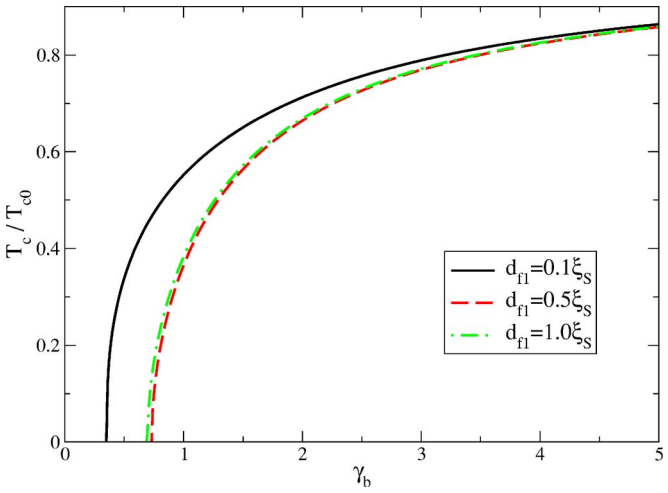

FIG. 4. (Color online) Critical temperature T_c of a trilayer versus the interface resistance parameter $\gamma_b=\gamma_{b1}=\gamma_{b2}$ at a few thicknesses d_{f1} corresponding to points on the $J=20T_{c0}$ curve in Fig. 2 to the left, inside, and to the right of the $T_c=0$ region. The model parameters are given in Table II.

In Fig. 6 we show the influence of the relative direction of the exchange fields in the two ferromagnetic layers. The dependence is monotonic, with the parallel orientation being the most destructive. We note (see also Refs. 10 and 14) that for parallel or antiparallel exchange field orientations triplet correlations with zero spin projection on the local exchange field are present in the structure, while for intermediate orientations triplet correlations with nonzero spin projection are also induced. In order to describe the θ dependence correctly,

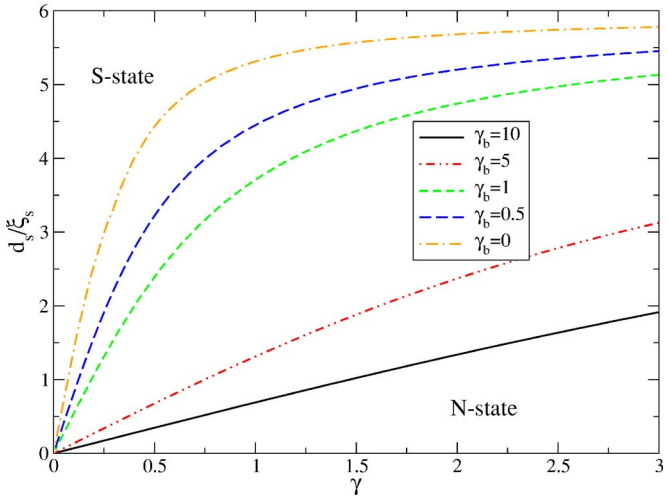

FIG. 5. (Color online) Critical thickness d_s for which $T_c \to 0$ versus the conductivity mismatch γ for a number of values of the interface resistance parameter γ_b. The lines separate the normal phase (below) from the superconducting phase (above). The model parameters are given in Table II.

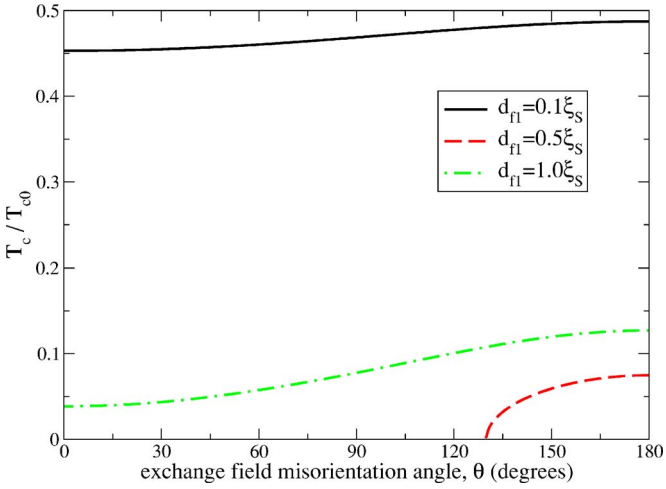

FIG. 6. (Color online) Critical temperature T_c of a trilayer versus the misorientation angle θ between the exchange fields in ferromagnets F_1 and F_2. The model parameters are given in Table II.

it is therefore important to include $\mathbf{f}_t$, see Appendix A.

In Fig. 7(a) we present order parameter profiles for four different values of γ_b on the solid line ($d_{f1}=0.1\xi_s$) in Fig. 4. For a good contact (small resistance γ_b), the pair breaking becomes quite severe. The suppression is reflected as a growth of the Fourier components $p \geqslant 1$, see Fig. 7(b).

IV. PENTALAYER

Consider the pentalayer shown in Fig. 8. Experimental results for the critical temperature, including signatures of a transition from a 0 junction to a π junction as function of the thickness of the central F layer, were recently presented for this structure in Ref. 32. The theory fits of T_c of the pentalayers in Ref. 32 were obtained with the theory presented in the present paper.

The superconducting layers are considered geometrically identical with identical bulk material critical temperatures T_{c0}. In the central ferromagnetic layer (F_1), the exchange field is aligned with the z axis, while in the right and left layers (F_2) it forms an angle θ with respect to the z axis. We characterize the different layers by their thicknesses, exchange fields, and diffusion constants, with the constraint that the pentalayer should have certain symmetries with respect to the midpoint, see below. The present pentalayer problem can then be reduced to a trilayer problem with a new effective boundary condition at a fictitious outer surface at the center ($x=0$). The two superconducting order parameters in the left and right S layers may differ in phase, which is reflected in the effective boundary condition.

We shall consider two types of misorientation of the exchange fields in the outer layers relative to the center layer: the exchange fields J_2 are rotated by $+\theta$ as in Fig. 4 (rotation type 1, $+\theta/+\theta$), or rotations by $-\theta$ and $+\theta$ in the left and right outer layers, respectively, (rotation type 2, $-\theta/+\theta$).

For rotation type 1 $(+\theta/+\theta)$, when the phase difference vanishes (0-junction case), the singlet component f_s is an even function of x. Considering the parity of the exchange field $\mathbf{J}$ ($J_z \to J_z$ and $J_y \to J_y$) and the Eqs. (1) and (2), we deduce that the f_{tz} and f_{ty} components have the same even parity. Thus, we impose the conditions

$$(+\theta, +\theta), 0-\text{jct}: f_s'(0) = f_{tz}'(0) = f_{ty}'(0) = 0. \tag{13}$$

On the other hand, when the phase difference is π (π-junction case), f_s, f_{tz}, and f_{ty} are odd functions of x and we impose the conditions

$$(+\theta, +\theta), \pi-\text{jct}: f_s(0) = f_{tz}(0) = f_{ty}(0) = 0. \tag{14}$$

For rotation type 2 $(-\theta/+\theta)$, the exchange field component J_y is instead odd under $x \to -x$. For the 0-junction case, it implies that f_{ty} is odd, while the other components are even just as above. For the π-junction case the parities are interchanged. The effective boundary conditions are

$$(-\theta/+\theta), 0-\text{jct}: \begin{cases} f_s'(0) = f_{tz}'(0) = 0, \\ f_{ty}(0) = 0, \end{cases} \tag{15}$$

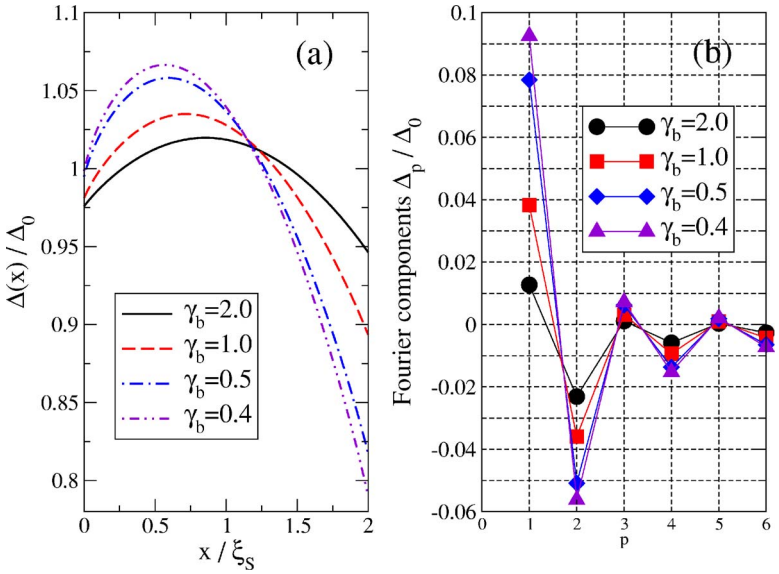

FIG. 7. (Color online) (a) The spatial dependence of the order parameter for several interface resistance parameters $\gamma_b=\gamma_{b1}=\gamma_{b2}$ on the solid curve ($d_{f1}=0.1\xi_s$) in Fig. 4. (b) The Fourier components in Eq. (10). Note that Δ is normalized to the first component Δ_0, which remains unknown in a linearized theory.

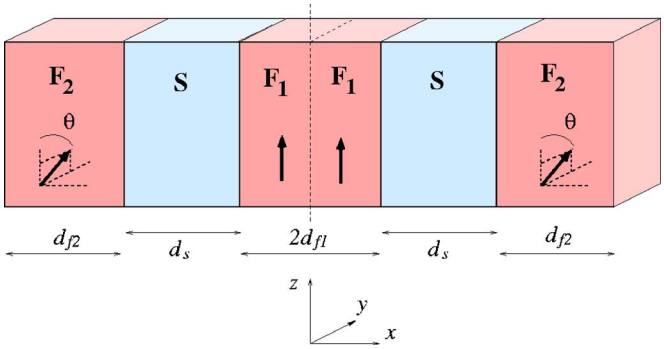

FIG. 8. (Color online) The $F_2/S/F_1/S/F_2$ pentalayer structure. We consider two types of misalignment of the outer exchange fields relative to the exchange field in the center layer. First, as shown here, J_2 is rotated by the same angle θ. The second possibility is when J_2 is rotated in opposite directions, $-\theta$ in the left F_2 and $+\theta$ in the right F_2.

$$(-\theta/+\theta),\pi-\text{jct:}\begin{cases} f_s(0)=f_{tz}(0)=0, \\ f'_{ty}(0)=0. \end{cases} \tag{16}$$

As shown in Appendix B, the different boundary conditions yield different matrices $\hat{W}$ for the effective boundary condition (6).

Results

The dependence of T_c on the various parameters in the model is similar for the trilayer with left ferromagnetic layer thickness d_{f1} and for the pentalayer with a phase difference 0 between the two superconductors and a central ferromagnet layer thickness $2d_{f1}$. The critical temperature is in fact equal for rotation type I, since the boundary condition at the center of the pentalayer, Eq. (13), is the same as for the outer surface of the trilayer. Note, however, that the boundary condition for one of the triplets is different for rotation type II, see Eq. (15). The new ingredient in the pentalayer case is the possibility of a phase difference π between the superconductors. The π state can in simplified terms be understood as being due to the oscillatory behavior of the Green's function

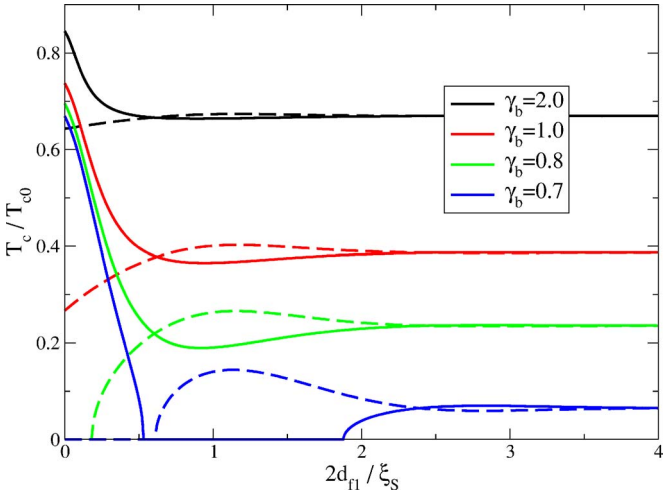

FIG. 9. (Color online) Critical temperature T_c of a pentalayer versus the center ferromagnet layer thickness $2d_{f1}$ for several barrier transparencies. The curves come in pairs, solid line for the 0 junction and dashed line for the π junction, from top to bottom for $\gamma_{b1}=\gamma_{b2}=\gamma_b=\{2,1,0.8,0.7\}$, respectively. The model parameters are given in Table III.

$f_s(\varepsilon_n,x)$ inside the central ferromagnetic layer F_1. In an experiment, T_c is given by the largest T_c for each thickness and there will be a sudden almost kink-like change in T_c at the $0\rightarrow\pi$ transition. For large oscillations, the transition becomes sharper. This is illustrated by changing the interface resistance γ_b in Fig. 9. (See Table III.) For good contacts and strong exchange fields, superconductivity can be destroyed at some critical thickness and then reappear at a larger thickness, just as in the trilayer case. For the pentalayer, however, the π phase can pre-empt the 0 phase and superconductivity appears earlier compared to the trilayer as d_{f1} is increased, see the curves for $\gamma_b=0.7$ in Fig. 9.

An example of the order parameter suppression is shown in Fig. 10(a), corresponding to $\gamma_b=0.8$ and $2d_{f1}=0.4\xi_s$ in Fig. 9. The suppression of Δ at the interfaces is more severe for phase difference π and the 0 junction is stabilized, i.e., has the largest T_c as seen in Fig. 9.

In the region close to the $0\rightarrow\pi$ transition, it is possible to switch between the 0 phase and π phase by changing the

TABLE III. Values for the model parameters used in Figs. 9–16. Note that $2d_{f1}$ denotes the center ferromagnetic thickness of the pentalayer shown in Fig. 8.

	Parameter values for the pentalayer						
Figure no.	d_s	$2d_{f1}$	d_{f2}	J	θ	γ	γ_b
9	2	~	0.5	20	0	0.3	~
10	2	0.4	0.5	20	0	0.3	0.8
11	2	~	0.5	20	~	0.3	0.8
12	2	~	0.5	20/10	~	0.3	0.8
13	2	~	0.2	10	~	0.35	0.4
14	2	~	0.5	10	0/90°	0.3	0.8
15	2	~	0.2	10	0	0.35	0.4
16	2	0.7	0.2	10	0	0.35	0.4

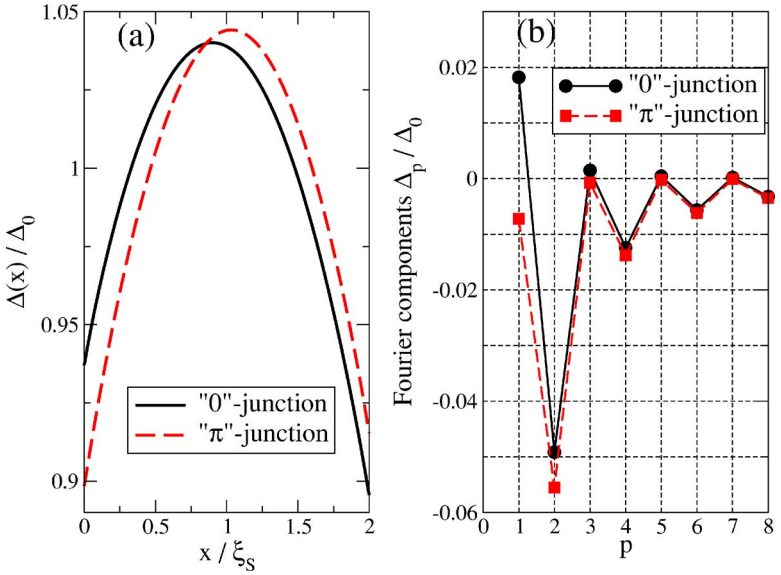

FIG. 10. (Color online) (a) The order parameter profile for the parameters in Fig. 9 for $\gamma_b=0.8$ at $2d_{f1}=0.4\xi_s$, for which the critical temperature for the 0 and π junctions are, respectively, $T_c \approx 0.3T_{c0}$ and $T_c=0.16T_{c0}$. (b) The corresponding Fourier components.

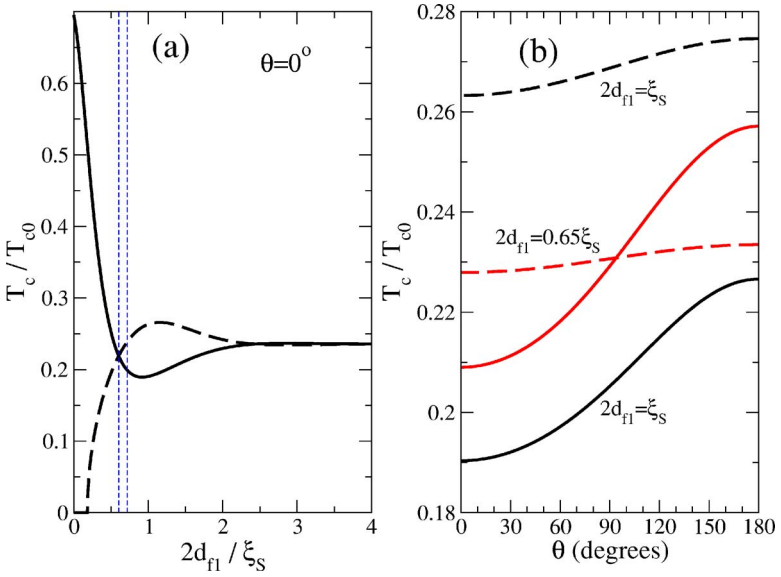

FIG. 11. (Color online) (a) The same curves as in Fig. 9 for $\gamma_b=0.8$. For thicknesses d_{f1} between the two vertical lines the $0\rightarrow\pi$ transition can be tuned by the relative orientation of the exchange fields in F_1 and F_2. (b) The switch $0\rightarrow\pi$ appears at a critical angle $\theta_c \approx 84°$ for the thickness $2d_{f1}=0.65\xi_s$. For the larger thickness $2d_{f1}=\xi_s$, outside the window indicated in (a), the largest T_c is obtained for the π-junction.

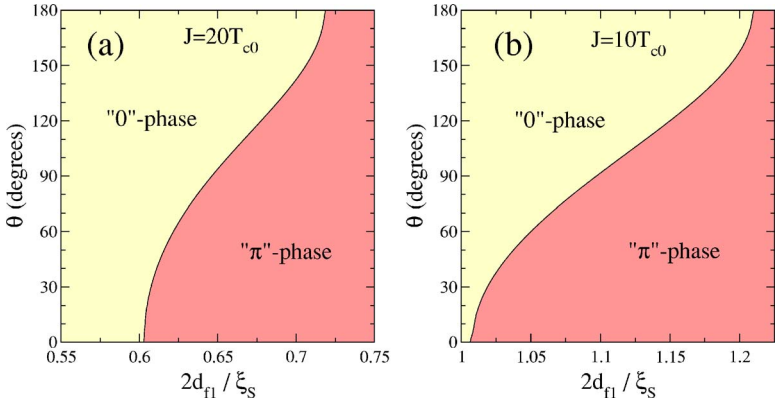

FIG. 12. (Color online) (a) Phase diagram of the $0\rightarrow\pi$ transition in the window indicated in Fig. 11(a). In (b) we show the phase diagram for a smaller exchange field, $J=10T_{c0}$. The range of thicknesses d_{f1} for which there is a switching by changing θ is larger in this case.

relative orientation of the exchange fields. We note that this possibility was already deduced from calculations of the Josephson critical current in Refs. 34 and 37 considering different geometries. We illustrate this effect in Fig. 11: switching is possible in between the vertical lines in Fig. 11(a). Since, experimentally, T_c is given by the largest T_c for each θ, the $0\rightarrow\pi$ switch would show up as a sudden almost kink-like change in T_c with the variation of θ, as shown in Fig. 11(b). We present in Fig. 12 the phase diagram of the junction in the region around the window indicated in Fig. 11(a). The window inside which a $0\rightarrow\pi$ phase change can be induced by the orientation angle θ is larger for a smaller exchange field since the T_c-oscillation period is longer in this case. We see this effect by comparing the $J=20T_{c0}$ case in Fig. 11(a) to the $J=10T_{c0}$ case shown in (b).

It has been found[8,9,24] for the bilayer and trilayer cases that T_c can become a multiple valued function of, e.g., the thickness of the ferromagnet. We show this type of behavior for the pentalayer case in Fig. 13(a). The nonmonotonic dependence of T_c is similar to the case of a clean thin film in an in-plane magnetic field[50,51] and to thin films of superfluid ^{3}He.[52,53] For these clean systems it has been proposed that an inhomogeneous superconducting state can be formed. In a dirty system, such inhomogeneity seems very unlikely and it has instead been proposed that the back-bend signals the possibility of a first-order transition in the system.[24] First-order transitions are, however, beyond the scope of the present paper. Instead we point out that for the pentalayer case, the π phase becomes favorable in the same region of thicknesses as where there is a back-bend for the 0 junction. The back-bend behavior for the 0 junction, and the interfering π phase, occurs also as function of the exchange field misorientation angle θ, see Fig. 13(b) Interestingly, there is a discontinuous drop in T_c at the $0\rightarrow\pi$ transition when θ is tuned from around 20° down to 10°, see the solid and dashed lines in Fig. 13(b). The competition between inhomogeneous states and the π state in ballistic S-F structures was studied very recently in Ref. 54.

For very large thicknesses d_{f1} the predominant superconducting correlations that penetrate F_1 and connect the two superconductors are the long-range nonoscillatory triplet components of $\mathbf{f}_t$. As a consequence, at large d_{f1}, T_c becomes a monotonic function of d_{f1}. The difference in T_c between the 0 and π phases is, however, very small, see Fig. 14. The junction is stabilized at large d_{f1} either at 0 or at π phase difference, depending on the way the exchange fields of the two outer ferromagnetic layers are rotated relative to the center layer (a similar effect associated with the chirality of the rotation has been found in Ref. 37 from calculations of the critical current in S-F multilayered junctions). When f_{ty} has odd parity it is smaller compared to the even parity case, which leads to a smaller suppression of the singlet f_s, i.e., less pair breaking, and a higher T_c. Thus, for rotation type 1 we have a π junction at large d_{f1} because f_{ty} has odd parity, see Fig. 14(a). On the other hand, for rotation type 2 we have a 0 junction at large d_{f1} because f_{fy} is odd for this rotation type and phase difference, see Fig. 14(b). We show the spatial dependence of the long range (in the central F_1 layer) triplet Green's function

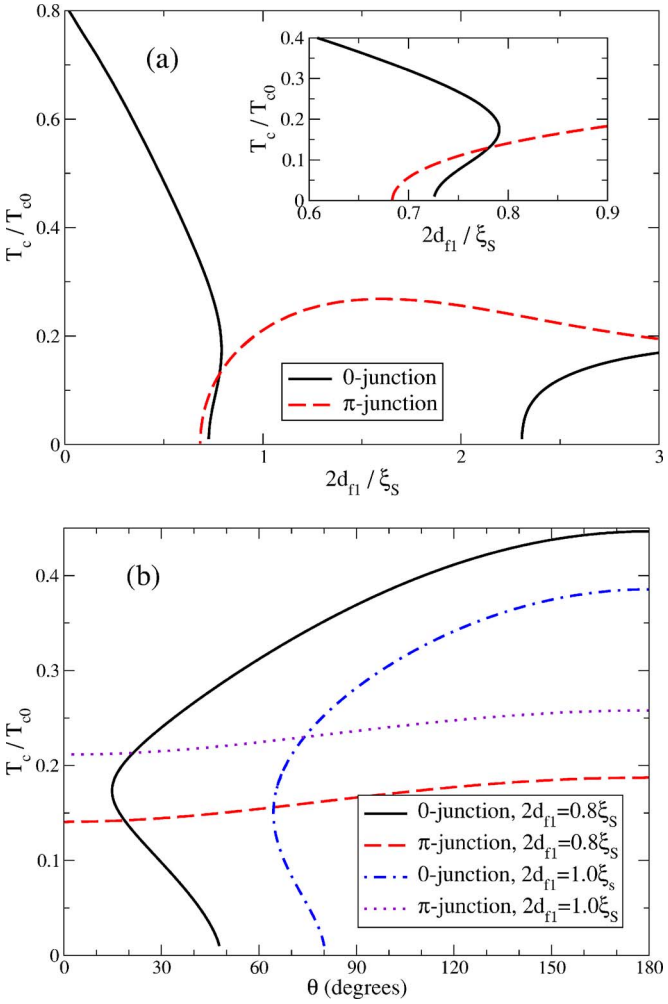

FIG. 13. (Color online) (a) Next to the region where T_c is suppressed to zero, the curve $T_c(d_{f1})$ can contain a back-bend. This latter could signal the occurrence of a first-order transition, which is, however, beyond the scope of the present theory. For the pentalayer, the π-phase can interfere and the first order transition might be avoided. In (b) we study the dependence on the exchange field misorientation angle θ for two particular thicknesses d_{f1} in (a). Clearly, the back-bend behavior can occur also as function of θ. The model parameters are given in Table III.

$$\Phi_{ty}(x) = T\sum_{\varepsilon_n>0} f_{ty}(\varepsilon_n,x) \tag{17}$$

in the inset of Fig. 14(b).

Experimentally, the transition from $0\rightarrow\pi$ was studied until now by varying the thickness[18,29–32] of the ferromagnet in S-F-S junctions, or by varying the temperature,[26–28] which is more practical since the transition is seen in the same device. Here we have studied another possibility to switch from the 0 to the π state within the same device, namely by continuously changing the relative orientation of the ferromagnetic moments. Our results are qualitatively consistent with the results obtained within Josephson critical current calculations.[34,37] The feasibility of controlling the orientation of the moments has been proven experimentally through the

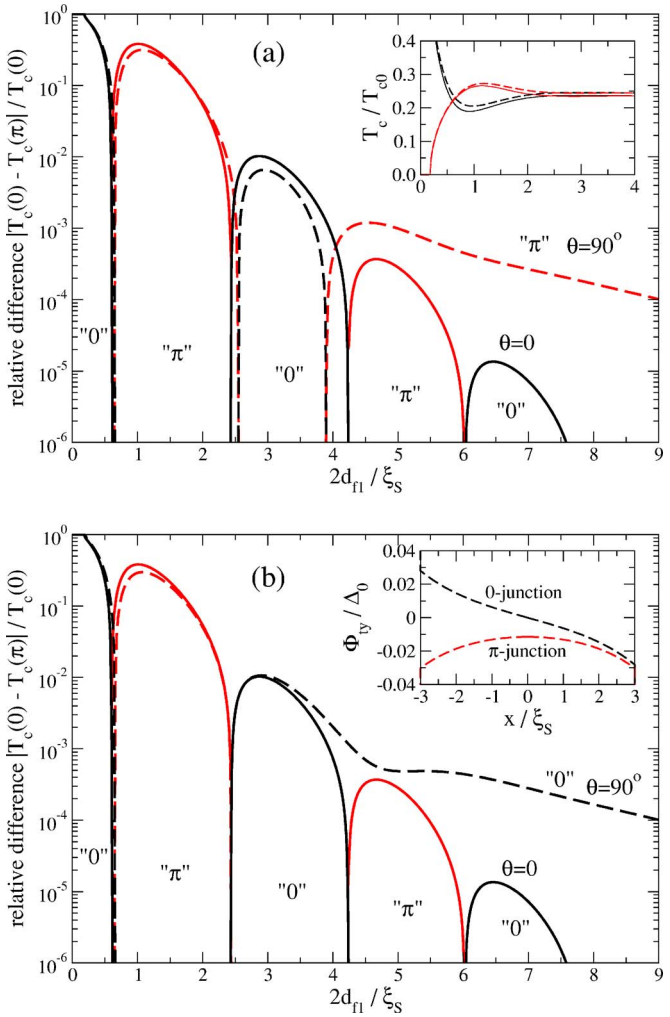

FIG. 14. (Color online) For thick center films (large d_{f1}) the communication between the two superconductors is taken over by long-range nonoscillatory equal spin triplet correlations and the junction is stabilized at phase difference 0 or π depending on the exchange field orientation: in (a) a π junction for $\theta=90°$ is obtained for exchange field rotation type 1 ($+\theta$ in both the left and right outer ferromagnets F_2, as illustrated in Fig. 8), while in (b) a 0 junction for $\theta=90°$ is obtained for rotation type 2 ($-\theta$ in the left F_2 and $+\theta$ in the right F_2). The difference in T_c between the 0 and π cases is quite small for large d_{f1}. For $\theta=0$ we use solid lines and for $\theta=90°$ we use dashed lines. Inset in (a): the differences in T_c for various exchange field orientations are due to the interaction between the ferromagnetic layers F_1 and F_2. Inset in (b): spatial dependence inside the central $6\xi_s$ thick F_1 layer of the long-range triplet f_{ty} induced for $\theta=90°$. The parameters are given in Table III.

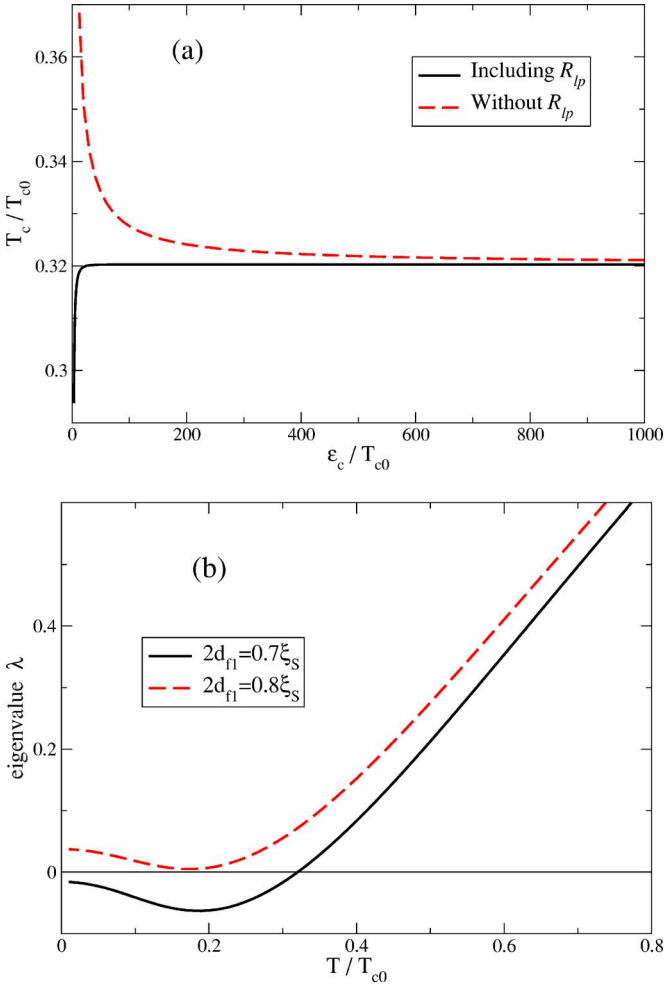

FIG. 15. (Color online) (a) Critical temperature versus the technical cutoff ε_c. To achieve good accuracy for the critical temperature we need ε_c of order $1000T_{c0}$ (dashed line). When the high-energy tail is summed to infinity, as described for the Fourier method in Eq. (F10), the convergence is more acceptable (solid line). (b) The eigenvalue of the gap equation (12) versus temperature for two different thicknesses. The zero-crossing determines T_c. When T_c is suppressed, $\lambda(T)$ can become a flat function of T which makes it important to compute λ with high accuracy to avoid numerical errors in T_c. The parameters in (a) were chosen as in Fig. 13, 0 junction, at $2d_{f1}=0.7$ and $\theta=0$. In (b) the two thicknesses are indicated in the legend. See also Table III.

investigation of F-S-F trilayers for different moment orientations.[16,20–22]

V. DISCUSSION OF THE NUMERICS

Let us discuss some delicate problems that need to be addressed when T_c is computed in inhomogeneous structures. In particular, we will compare the two methods of computing T_c: Eq. (12) which we call the Fourier method and Eq. (9) which we call the grid method.

The most important problem to address in any calculation using Usadel's approximation is the fact that the Matsubara sum in Eq. (5) is intrinsically slowly convergent, as compared to calculations done with the more general Eilenberger approach. As we show in Appendix E, the difference $f_s(\varepsilon_n) - \pi\Delta/|\varepsilon_n|$ appearing in the gap equation (5) is at high energies proportional to $1/\varepsilon_n^2$ for inhomogeneous systems. This can be contrasted with an Eilenberger approach, where the high-energy asymptotic is $1/|\varepsilon_n|^3$. It is therefore always necessary to extend the Matsubara sum to high energies when the Usadel approximation is employed, see the dashed line in Fig. 15(a). In the example we need a technical cutoff of order $1000T_{c0}$ to compute T_c with an accuracy of 1%. However, since the high-energy form of $f_s(\varepsilon_n)$ is known (see Appendix

E) it is in principle possible to circumvent the problem by treating the high-energy tail separately and sum the Matsubara sum to infinity. We have done that within the Fourier series approach, see Appendix F. A more acceptable cutoff of order $100T_c$ is then enough to achieve excellent accuracy, see the solid line in Fig. 15(a).

There are several other factors that, together with the slow convergence of the Matsubara sum, conspire to make it nontrivial to achieve acceptable accuracy, especially when T_c is small compared to T_{c0}. The critical temperature is computed by finding the temperature for which the eigenvalue λ of the gap equation is zero [Fourier method, Eq. (12)] or one [grid method, Eq. (9)]. The function $\lambda(T)$ can become a very flat function of T in the region where T_{c0} is small, see Fig. 15(b). Any error made in the calculation of λ can therefore be magnified to a larger error in T_c and it becomes increasingly critical to compute λ with high accuracy as T_c is suppressed.

The above two technical problems are particularly hard to circumvent within the grid method. First of all, the need to include high energies up to a technical cutoff ε_c imposes a condition on the grid spacing δx. At high energies the function $G(\varepsilon_n,x,y)$ is typically peaked in the region $x\sim y$:

$$G(\varepsilon_n \gg T_{c0},x,y) \sim \frac{k_s(\varepsilon_n)}{\varepsilon_n} e^{-k_s(\varepsilon_n)|x-y|}, \tag{18}$$

where $k_s(\varepsilon_n)=\sqrt{2\varepsilon_n/D}$. It is therefore necessary to choose

$$\frac{\delta x}{\xi_s} \ll \frac{1}{\xi_s k_s(\varepsilon_c)} = \sqrt{\frac{\pi T_{c0}}{\varepsilon_c}}, \tag{19}$$

to resolve this dependence. Since we need a cutoff around $1000T_{c0}$, because of the slow convergence within the Usadel approach, we need a grid spacing of order $0.01\xi_s$ or finer. The matrix in Eq. (9) must therefore typically be of the order of a few hundred elements square, which severely slows down the numerics.

One reason for the importance to resolve the peaked form of $G(\varepsilon_n,x,y)$ is due to the interchange in order of the Matsubara sum and the integration over y in Eq. (9). We write Eq. (9) as

$$\int_0^{d_s} K(x,y)\Delta(y)dy = \Delta(x), \tag{20}$$

and compute each element of the matrix $K(x,y)$ by summing over ε_n. The asymptotic form of the diagonal is, however, $G(\varepsilon_n,x,x)\propto 1/\sqrt{\varepsilon_n}$ and the Matsubara sum is not convergent. This is in principle irrelevant for the calculation of T_c because T_c only depends on the eigenvalue of the matrix, which is a quantity given by the Matsubara sum integrated over y. Note that when Eq. (18) is integrated over y, a factor $1/k_s$ appears in the primitive function of the exponential and the asymptotic form is $1/|\varepsilon_n|$, which is (by construction) canceled by the sum over $1/|\varepsilon_n|$ in the denominator of $K(x,y)$, see Eq. (9). Numerically, however, the integral over the discretized coordinate y can only be computed with some accuracy given by the grid spacing δx. The error made in computing the integral is transferred into an error in the eigenvalue λ which, as described above, can result in an error in T_c magnified by the flatness of the $\lambda(T)$ dependence.

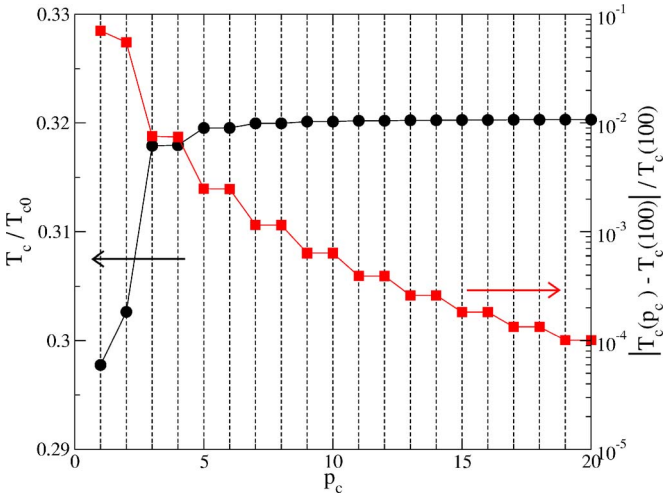

FIG. 16. (Color online) Critical temperature versus the number p_c of included Fourier coefficients in Eq. (10). The variation in absolute numbers is shown by circles (vertical scale to the left), while the variation in relation to the corresponding value for T_c at a high cutoff $p_c=100$ is shown by squares (vertical scale to the right). The even-odd variation is due to the choice of parameters: the junction is almost symmetric and the even-number Fourier components corresponding to symmetric cos functions contribute more to T_c. The model parameters were chosen as in Fig. 15, upper panel (see also Table III).

To circumvent the problems described above, one must predict the high-energy tail to avoid cutoffs larger than $\sim 100T_{c0}$. Within the grid method that means computing the derivative of $\Delta(x)$, i.e., to introduce an approximate formula for the derivative on a discretized grid. But that also introduces numerical errors and the grid must still be dense, which means that the matrix $K(x,y)$ remains large and the calculation with the grid method is always very slow and susceptible to numerical errors.

All the problems related to the discretization of the spatial coordinate are avoided within the Fourier series approach, since $G(\varepsilon_n,x,y)$ is analytically integrated over x and y in the course of the derivation of the matrix m_{lp} in Eq. (12), see Appendix D. Moreover, the high-energy tail is easily predicted analytically, see Appendix F. It is typically sufficient to include only the 20 first Fourier components in the calculation of T_c, see Fig. 16. The matrix m_{lp} is therefore small, the high-energy cutoff of the Matsubara sum can be chosen reasonably small, and very high accuracy is achieved while the speed of the calculation remains very high.

VI. SUMMARY

In conclusion, we have studied the change of the superconducting critical temperature T_c in asymmetric trilayers F_1-S-F_2 and symmetric pentalayers F_2-S-F_1-S-F_2 with any relative orientation angle between the magnetizations of F_1 and F_2. For both cases we have presented phase diagrams, showing T_c as function of the misorientation angle θ, and as a function of the ferromagnet layer thicknesses. We have

investigated the interplay of long-range triplet components and Josephson coupling in the pentalayer geometry. We have demonstrated the possibility to switch between the 0 and π states by controlling the relative orientation of the F moments in a pentalayer structure. This behavior may be appealing for the experimental study of the $0 \rightarrow \pi$ transition. We have presented details of a general method for the computation of T_c and the spatial dependence of the order parameter in diffusive hybrid structures with weak exchange fields $J\tau \ll 1$. With this technique, the accuracy, as well as the speed of the numerics, are immensely improved compared with previously used techniques.

ACKNOWLEDGMENTS

We acknowledge support from the Deutsche Forschungsgemeinschaft within the Center for Functional Nanostructures (T.C. and M.E.), and the Alexander von Humboldt Foundation (T.L.).

APPENDIX A: DERIVATION OF $\hat{W}$ FOR THE TRILAYER

In this appendix we provide the details of the calculations leading to the effective boundary condition (6) obeyed by the singlet component in the superconducting region in asymmetric F_1-S-F_2 trilayers with an arbitrary mutual orientation between the magnetizations in F_1 and F_2. Except for this latter component, it is possible to derive analytically the spatial dependences of all the components of the anomalous Green's function f close to T_c (next section). In Sec. A 2 we determine from the consideration of the boundary conditions (3) and (4) the matrix $\hat{W}$ that enters the expression for the effective boundary condition (6).

1. Spatial dependences

In the superconducting layer, the triplet vector $\mathbf{f}_t$ obeys a homogeneous differential equation [Eq. (2) with $\mathbf{J}=\mathbf{0}$] which is straightforwardly solved:

$$\mathbf{f}_t = \mathbf{c}\cosh(k_s x) + \mathbf{d}\sinh(k_s x) \tag{A1}$$

with $\mathbf{c}$ and $\mathbf{d}$ constants.

For a fixed exchange field in each F layer, the system of coupled Eqs. (1) and (2) can be easily solved in the ferromagnetic regions. After application of the boundary conditions at the outer surfaces, the solutions can be written in the form[42]

$$\begin{pmatrix} f_s \\ \mathbf{f}_t \end{pmatrix} = \sum_{\varepsilon=\pm} a_\varepsilon \cosh[k_{\varepsilon 1}(x+d_{f1})] \begin{pmatrix} 1 \\ \varepsilon\hat{\mathbf{z}} \end{pmatrix} + a_0 \cosh[k_{01}(x+d_{f1})] \begin{pmatrix} 0 \\ \hat{\mathbf{y}} \end{pmatrix} \tag{A2}$$

for the F_1 layer, and

$$\begin{pmatrix} f_s \\ \mathbf{f}_t \end{pmatrix} = \sum_{\varepsilon=\pm} b_\varepsilon \cosh[k_{\varepsilon 2}(x-d_s-d_{f2})] \begin{pmatrix} 1 \\ \varepsilon(\cos\theta\hat{\mathbf{z}} + \sin\theta\hat{\mathbf{y}}) \end{pmatrix} + b_0 \cosh[k_{02}(x-d_s-d_{f2})] \begin{pmatrix} 0 \\ \sin\theta\hat{\mathbf{z}} - \cos\theta\hat{\mathbf{y}} \end{pmatrix} \tag{A3}$$

for the F_2 layer. Here we have defined

$$k_{\pm q} = \sqrt{(2\varepsilon_n \pm 2iJ_q)/D_{fq}}, \tag{A4}$$

$$k_{0q} = \sqrt{2\varepsilon_n/D_{fq}}, \tag{A5}$$

with the index $q=1$ or 2 referring to the F_1 or F_2 layer.

2. Determination of $\hat{W}$

The constants a_j and b_j ($j=\pm,0$), $\mathbf{c}$, and $\mathbf{d}$ are determined with the help of the boundary conditions (3) and (4) considered for the two S/F interfaces. Writing these conditions for the triplet components only, we have

$$\xi_s f_l'(x_{Sq}) = \gamma_q \xi_{fq} f_l'(x_{Fq}), \tag{A6}$$

$$f_l(x_{Sq}) = f_l(x_{Fq}) + \eta_q \gamma_{bq} \xi_{fq} f_l'(x_{Fq}), \tag{A7}$$

with $l=t_y,t_z$. Note that $\eta_1=+1$ and $\eta_2=-1$. Similarly, we get for the singlet amplitude

$$\xi_s f_s'(x_{Sq}) = \gamma_q \xi_{fq} f_s'(x_{Fq}), \tag{A8}$$

$$f_s(x_{Sq}) = f_s(x_{Fq}) + \eta_q \gamma_{bq} \xi_{fq} f_s'(x_{Fq}). \tag{A9}$$

Here, x_{F1} and x_{S1} are the coordinates on the two sides of the F_1/S interface at $x_1=0$, while x_{F2} and x_{S2} refers to the S/F_2 interface at $x_2=d_s$. From Eqs. (A9) and (A7) for the first interface (F_1/S), we obtain the system

$$f_s(x_1) = \sum_{\varepsilon=\pm} a_\varepsilon \mathcal{A}_\varepsilon, \tag{A10}$$

$$c_y = a_0 \mathcal{A}_0, \tag{A11}$$

$$c_z = \sum_{\varepsilon=\pm} \varepsilon a_\varepsilon \mathcal{A}_\varepsilon, \tag{A12}$$

with the quantity

$$\mathcal{A}_j = \cosh(k_{j1}d_{f1}) + \gamma_{b1} k_{j1} \xi_{f1} \sinh(k_{j1}d_{f1}), \tag{A13}$$

where $j=\pm,0$. The matching of the different components with the conditions (A9) and (A7) yields at the second interface (S/F_2)

$$f_s(x_2) = \sum_{\varepsilon=\pm} b_\varepsilon \mathcal{B}_\varepsilon, \tag{A14}$$

$$c_y \cosh(k_s d_s) + d_y \sinh(k_s d_s) = \sum_{\varepsilon=\pm} \varepsilon b_\varepsilon \mathcal{B}_\varepsilon \sin\theta - b_0 \mathcal{B}_0 \cos\theta, \tag{A15}$$

$$c_z \cosh(k_s d_s) + d_z \sinh(k_s d_s) = \sum_{\varepsilon=\pm} \varepsilon b_\varepsilon \mathcal{B}_\varepsilon \cos\theta + b_0 \mathcal{B}_0 \sin\theta, \tag{A16}$$

with

$$\mathcal{B}_j = \cosh(k_{j2} d_{f2}) + \gamma_{b2} k_{j2} \xi_{f2} \sinh(k_{j2} d_{f2}) \tag{A17}$$

defined in a similar way as the quantity $\mathcal{A}_j$. Then, the boundary conditions (A6) yield the system

$$d_y = a_0 \mathcal{C}_0, \tag{A18}$$

$$d_z = \sum_{\varepsilon=\pm} \varepsilon a_\varepsilon \mathcal{C}_\varepsilon, \tag{A19}$$

for the F_1/S interface, and

$$c_y \sinh(k_s d_s) + d_y \cosh(k_s d_s) = b_0 \mathcal{D}_0 \cos\theta - \sum_{\varepsilon=\pm} \varepsilon b_\varepsilon \mathcal{D}_\varepsilon \sin\theta, \tag{A20}$$

$$c_z \sinh(k_s d_s) + d_z \cosh(k_s d_s) = -b_0 \mathcal{D}_0 \sin\theta - \sum_{\varepsilon=\pm} \varepsilon b_\varepsilon \mathcal{D}_\varepsilon \cos\theta, \tag{A21}$$

for the S/F_2 interface, with

$$\mathcal{C}_j = \gamma_1 k_{j1} \xi_{f1} \sinh(k_{j1} d_{f1})/k_s \xi_s, \tag{A22}$$

$$\mathcal{D}_j = \gamma_2 k_{j2} \xi_{f2} \sinh(k_{j2} d_{f2})/k_s \xi_s. \tag{A23}$$

The next step consists of eliminating the coefficients $c_y, c_z, d_y, d_z, a_0, b_0$ from the former equations. We obtain the system

$$\sum_\varepsilon \varepsilon a_\varepsilon \mathcal{E}_\varepsilon = \sum_\varepsilon \varepsilon b_\varepsilon \mathcal{G}_\varepsilon, \tag{A24}$$

$$\sum_\varepsilon \varepsilon b_\varepsilon \mathcal{F}_\varepsilon = \sum_\varepsilon \varepsilon a_\varepsilon \mathcal{H}_\varepsilon, \tag{A25}$$

where

$$\mathcal{E}_\varepsilon = K_0(\mathcal{A}_\varepsilon - \mathcal{C}_\varepsilon)[\cosh(k_s d_s) - \sinh(k_s d_s)]\cos\theta, \tag{A26}$$

$$\mathcal{F}_\varepsilon = K_\varepsilon(\mathcal{B}_0 - \mathcal{D}_0)\sin^2\theta + K_0(\mathcal{B}_\varepsilon - \mathcal{D}_\varepsilon)\cos^2\theta, \tag{A27}$$

$$\mathcal{G}_\varepsilon = K_\varepsilon(\mathcal{B}_0 + \mathcal{D}_0)\sin^2\theta + K_0(\mathcal{B}_\varepsilon + \mathcal{D}_\varepsilon)\cos^2\theta, \tag{A28}$$

$$\mathcal{H}_\varepsilon = K_0(\mathcal{A}_\varepsilon + \mathcal{C}_\varepsilon)[\cosh(k_s d_s) + \sinh(k_s d_s)]\cos\theta, \tag{A29}$$

with

$$K_j = [\mathcal{B}_j \mathcal{C}_0 + \mathcal{D}_j \mathcal{A}_0]\cosh(k_s d_s) + [\mathcal{B}_j \mathcal{A}_0 + \mathcal{D}_j \mathcal{C}_0]\sinh(k_s d_s). \tag{A30}$$

Compiling Eqs. (A10) and (A14) with Eqs. (A24) and (A25), we get the expressions for the amplitudes a_ε and b_ε

$$a_\varepsilon = \frac{(\mathcal{B}_+ \mathcal{I}_{-,-\varepsilon} + \mathcal{B}_- \mathcal{I}_{+,-\varepsilon}) f_s(x_1) + \varepsilon \mathcal{A}_{-\varepsilon}(\mathcal{F}_- \mathcal{G}_+ - \mathcal{F}_+ \mathcal{G}_-) f_s(x_2)}{\mathcal{J}}, \tag{A31}$$

$$b_\varepsilon = \frac{(\mathcal{A}_+ \mathcal{I}_{-\varepsilon,-} + \mathcal{A}_- \mathcal{I}_{-\varepsilon,+}) f_s(x_2) + \varepsilon \mathcal{B}_{-\varepsilon}(\mathcal{E}_- \mathcal{H}_+ - \mathcal{E}_+ \mathcal{H}_-) f_s(x_1)}{\mathcal{J}}, \tag{A32}$$

with

$$\mathcal{I}_{\varepsilon,\varepsilon'} = \mathcal{F}_\varepsilon \mathcal{E}_{\varepsilon'} - \mathcal{G}_\varepsilon \mathcal{H}_{\varepsilon'}, \tag{A33}$$

$$\mathcal{J} = \mathcal{A}_+ \mathcal{B}_+ \mathcal{I}_{-,-} + \mathcal{A}_- \mathcal{B}_- \mathcal{I}_{+,+} + \mathcal{A}_+ \mathcal{B}_- \mathcal{I}_{+,-} + \mathcal{A}_- \mathcal{B}_+ \mathcal{I}_{-,+}. \tag{A34}$$

Finally, Eq. (A8) yields the system

$$\xi_s f_s'(x_1) = k_s \xi_s \sum_\varepsilon a_\varepsilon \mathcal{C}_\varepsilon, \tag{A35}$$

$$\xi_s f_s'(x_2) = -k_s \xi_s \sum_\varepsilon b_\varepsilon \mathcal{D}_\varepsilon, \tag{A36}$$

which can be rewritten in the form

$$\begin{pmatrix} f_s'(x_1) \\ f_s'(x_2) \end{pmatrix} = k_s \begin{pmatrix} W_{11} & W_{12} \\ W_{21} & W_{22} \end{pmatrix} \begin{pmatrix} f_s(x_1) \\ f_s(x_2) \end{pmatrix}, \tag{A37}$$

with

$$W_{11} = \frac{\mathcal{C}_+(\mathcal{B}_+ \mathcal{I}_{-,-} + \mathcal{B}_- \mathcal{I}_{+,-}) + \mathcal{C}_-(\mathcal{B}_+ \mathcal{I}_{-,+} + \mathcal{B}_- \mathcal{I}_{+,+})}{\mathcal{J}}, \tag{A38}$$

$$W_{22} = -\frac{\mathcal{D}_+(\mathcal{A}_+ \mathcal{I}_{-,-} + \mathcal{A}_- \mathcal{I}_{-,+}) + \mathcal{D}_-(\mathcal{A}_+ \mathcal{I}_{+,-} + \mathcal{A}_- \mathcal{I}_{+,+})}{\mathcal{J}}, \tag{A39}$$

$$W_{12} = \frac{(\mathcal{F}_- \mathcal{G}_+ - \mathcal{F}_+ \mathcal{G}_-)(\mathcal{A}_- \mathcal{C}_+ - \mathcal{A}_+ \mathcal{C}_-)}{\mathcal{J}}, \tag{A40}$$

$$W_{21} = -\frac{(\mathcal{E}_- \mathcal{H}_+ - \mathcal{E}_+ \mathcal{H}_-)(\mathcal{B}_- \mathcal{D}_+ - \mathcal{B}_+ \mathcal{D}_-)}{\mathcal{J}}. \tag{A41}$$

Using the expressions (A26)–(A29), one can notice that in fact $W_{12} = -W_{21}$ with

$$W_{12} = \frac{2K_0^2 \cos^2\theta (\mathcal{B}_- \mathcal{D}_+ - \mathcal{B}_+ \mathcal{D}_-)(\mathcal{A}_- \mathcal{C}_+ - \mathcal{A}_+ \mathcal{C}_-)}{\mathcal{J}}. \tag{A42}$$

For an asymmetric trilayer F_1-S-F_2, the diagonal coefficients W_{11} and W_{22} of the matrix $\hat{W}$ differ in general. In the special case of a symmetric trilayer F_1-S-F_1, we have $W_{11} = W_{22}$.

APPENDIX B: DERIVATION OF $\hat{W}$ FOR THE PENTALAYER

Due to the symmetry of the geometry, we need to determine the components of the anomalous Green function f only in half of the pentalayer, e.g., in the domain $x>0$. The problem is mapped back onto the asymmetrical F_1-S-F_2 trilayer problem previously considered in Appendix A. Because we have chosen a different origin for the system of coordinates, the F_1/S and S/F_2 interfaces are now located at the positions $x_1=d_{f1}$ and $x_2=d_s+d_{f1}$. Due to the shift in coordinates, we have used the expressions (A1) in the S layer and (A3) in the F_2 layer with x replaced by $x-d_{f1}$.

For the rotation type 1, the spatial dependences of the singlet and triplet components of f in the left F_1 layer are in the 0-junction case the same as in Eq. (A2) after the shift of coordinate. In the π-junction case, the boundary conditions at the (fictitious) outer surface $x=0$ have changed, and the spatial dependences in F_1 are now given by

$$\begin{pmatrix} f_s \\ \mathbf{f}_t \end{pmatrix} = \sum_{\varepsilon=\pm} a_\varepsilon \sinh[k_{\varepsilon 1}x] \begin{pmatrix} 1 \\ \varepsilon\hat{\mathbf{z}} \end{pmatrix} + a_0 \sinh[k_{01}x] \begin{pmatrix} 0 \\ \hat{\mathbf{x}} \end{pmatrix}.$$

The new boundary conditions (13) and (14) at $x=0$ do not affect the definition of the former quantities $\mathcal{B}_j$ and $\mathcal{D}_j$. On the other hand, changes occur in the definition of the quantities $\mathcal{A}_j$ and $\mathcal{C}_j$ (where $j=\varepsilon$ or 0). In the 0-junction case, the coefficients $\mathcal{A}_j$ and $\mathcal{C}_j$ remain unchanged, while in the π-junction case they are defined as

$$\mathcal{A}_j = \sinh(k_{j1}d_{f1}) + \gamma_{b1}k_{j1}\xi_{f1}\cosh(k_{j1}d_{f1}), \tag{B1}$$

$$\mathcal{C}_j = \gamma_1 k_{j1}\xi_{f1}\cosh(k_{j1}d_{f1})/k_s\xi_s. \tag{B2}$$

For the rotation type 2, the components of f in F_1 have a different spatial dependence as a result of the conditions (15) or (16). They are expressed as

$$\begin{pmatrix} f_s \\ \mathbf{f}_t \end{pmatrix} = \sum_{\varepsilon=\pm} a_\varepsilon \cosh[k_{\varepsilon 1}x] \begin{pmatrix} 1 \\ \varepsilon\hat{\mathbf{z}} \end{pmatrix} + a_0 \sinh[k_{01}x] \begin{pmatrix} 0 \\ \hat{\mathbf{x}} \end{pmatrix}$$

in the 0-junction case, and

$$\begin{pmatrix} f_s \\ \mathbf{f}_t \end{pmatrix} = \sum_{\varepsilon=\pm} a_\varepsilon \sinh[k_{\varepsilon 1}x] \begin{pmatrix} 1 \\ \varepsilon\hat{\mathbf{z}} \end{pmatrix} + a_0 \cosh[k_{01}x] \begin{pmatrix} 0 \\ \hat{\mathbf{x}} \end{pmatrix}$$

in the π-junction case. As for rotation type 1, changes occur in the definition of the quantities $\mathcal{A}_j$ and $\mathcal{C}_j$ (where $j=\varepsilon$ or 0) for the rotation type 2. In the 0-junction case, the coefficients $\mathcal{A}_\varepsilon$ and $\mathcal{C}_\varepsilon$ have the same expression as in Appendix A, while $\mathcal{A}_0$ and $\mathcal{C}_0$ are now given by

$$\mathcal{A}_0 = \sinh(k_{01}d_{f1}) + \gamma_{b1}k_{j1}\xi_{f1}\cosh(k_{01}d_{f1}), \tag{B3}$$

$$\mathcal{C}_0 = \gamma_1 k_{01}\xi_{f1}\cosh(k_{01}d_{f1})/k_s\xi_s. \tag{B4}$$

In the π-junction case, the quantities $\mathcal{A}_0$ and $\mathcal{C}_0$ are defined in the same way as in Appendix A, while $\mathcal{A}_\varepsilon$ and $\mathcal{C}_\varepsilon$ are written as

$$\mathcal{A}_\varepsilon = \sinh(k_{\varepsilon 1}d_{f1}) + \gamma_{b1}k_{\varepsilon 1}\xi_{f1}\cosh(k_{01}d_{f1}), \tag{B5}$$

$$\mathcal{C}_\varepsilon = \gamma_1 k_{\varepsilon 1}\xi_{f1}\cosh(k_{\varepsilon 1}d_{f1})/k_s\xi_s. \tag{B6}$$

Except for these modifications in the definition of the quantities $\mathcal{A}$ and $\mathcal{C}$, the remaining calculations are exactly the same as in the asymmetric trilayer geometry and we can use the final expression derived in Appendix A for the matrix $\hat{W}$ in the symmetric pentalayer structure.

APPENDIX C: DERIVATION OF $G(\varepsilon_n,x,y)$

In analogy with Ref. 8, Eq. (8) is solved by making the following ansatz:

$$G(x,y) = \begin{cases} L_c(y)X_1(x) + L_s(y)X_2(x), & x<y, \\ R_c(y)Y_1(x) + R_s(y)Y_2(x), & y<x, \end{cases} \tag{C1}$$

where we introduced the notation

$$X_1(x) = \cosh(k_s x), \tag{C2}$$

$$X_2(x) = \sinh(k_s x), \tag{C3}$$

$$Y_1(x) = \cosh(k_s[x-d_s]), \tag{C4}$$

$$Y_2(x) = \sinh(k_s[x-d_s]). \tag{C5}$$

The coefficients L_c, L_s, R_c, and R_s depend on the location y of the source term in Eq. (8). The source is taken into account by the conditions

$$G(x,y)|_{x=y^+} = G(x,y)|_{x=y^-} \tag{C6}$$

and

$$\partial_x G(x,y)|_{x=y^+} - \partial_x G(x,y)|_{x=y^-} = -k_s^2/\varepsilon_n, \tag{C7}$$

where y^+ and y^- denote the limits $y\to x$ from above and below, respectively. Equations (C6) and (C7) give two relations between the coefficients in Eq. (C1). Two additional relations are provided by the boundary conditions at the edges of the superconductor, which read

$$\begin{pmatrix} \partial_x G(x,y)|_{x=0} \\ \partial_x G(x,y)|_{x=d_s} \end{pmatrix} = k_s \hat{W} \begin{pmatrix} G(0,y) \\ G(d_s,y) \end{pmatrix}. \tag{C8}$$

These conditions are consistent with the boundary conditions (6) obeyed by the singlet amplitude $f_s(x)$. Compiling Eqs. (C1)–(C8), we obtain the coefficients

$$L_c(y) = \frac{k_s}{\varepsilon_n \mathcal{L}}[Y_1(y) + W_{22}Y_2(y) - W_{12}X_2(y)],$$

$$R_c(y) = \frac{k_s}{\varepsilon_n \mathcal{L}}[X_1(y) - W_{21}Y_2(y) + W_{11}X_2(y)],$$

$$L_s(y) = \frac{k_s}{\varepsilon_n \mathcal{L}}[W_{11}Y_1(y) + W_{12}X_1(y) + \det(\hat{W})Y_2(y)],$$

$$R_s(y) = \frac{k_s}{\varepsilon_n \mathcal{L}}[W_{21}Y_1(y) + W_{22}X_1(y) + \det(\hat{W})X_2(y)],$$

where

$$\mathcal{L} = W_{12} - W_{21} + (W_{11} - W_{22})\cosh(k_s d_s) + [1 - \det(\hat{W})]\sinh(k_s d_s).$$

We note that the dependence on the Matsubara frequency ε_n enters through k_s and the four elements W_{11}, W_{22}, W_{12}, and W_{22} of the 2×2 matrix $\hat{W}$ in the boundary condition.

APPENDIX D: DERIVATION OF m_{lp} IN EQ. (12)

We insert the expansion (10) into Eq. (7), use the expression for $G(\varepsilon_n, x, y)$ derived in Appendix C, and perform the integration over the spatial coordinate y. We obtain the singlet amplitude $f_s(\varepsilon_n, x)$ in terms of the Fourier coefficients Δ_p:

$$f_s(\varepsilon_n, x) = \frac{\pi}{\varepsilon_n \mathcal{L}} \sum_{p=0}^{\infty} \Delta_p \beta_p \left\{ \mathcal{L} \cos\left(\frac{\pi p x}{d_s}\right) + [W_{21} + (-1)^p W_{22}] X_1(x) - [W_{11} + (-1)^p W_{12}] Y_1(x) + \det(\hat{W})[(-1)^p X_2(x) - Y_2(x)] \right\}, \quad \text{(D1)}$$

where $\beta_p = 1/[1 + (\pi p / k_s d_s)^2]$ and the functions $\mathcal{L}$, $X_1(x)$, $X_2(x)$, $Y_1(x)$, and $Y_2(x)$ were introduced in Appendix C. We insert this expression in the gap equation (9) and project in Fourier space, i.e., we multiply by $\cos(\pi l x / d_s)$ and integrate over x. As a result, we obtain a linear system for the Fourier components Δ_p, with row $l \geqslant 0$ given by

$$\sum_{p=0}^{+\infty} m_{lp} \Delta_p = 0. \quad \text{(D2)}$$

The off-diagonal elements ($l \neq p$) have the form

$$m_{lp} = 4\pi T \sum_{\varepsilon_n > 0} \frac{1}{\varepsilon_n} b_{lp} \beta_l \beta_p, \quad \text{(D3)}$$

while the diagonal elements ($l = p$) are given by

$$m_{ll} = (1 + \delta_{l0}) \ln \frac{T}{T_{c0}} + 4\pi T \sum_{\varepsilon_n > 0} \frac{1}{\varepsilon_n} \left[b_{ll} \beta_l^2 + \frac{1}{2}(1 - \beta_l) \right], \quad \text{(D4)}$$

where

$$b_{lp} = \frac{[W_{11} - (-1)^{l+p} W_{22} + (-1)^p W_{12} - (-1)^l W_{21}]\sinh(k_s d_s) + \det(\hat{W})\{(-1)^p + (-1)^l - [1 + (-1)^{l+p}]\cosh(k_s d_s)\}}{k_s d_s \mathcal{L}}. \quad \text{(D5)}$$

The relation $W_{12} = -W_{21}$ between the off-diagonal elements of $\hat{W}$ found in Appendix A implies that the matrix $\hat{m}$ is symmetric, i.e., $m_{lp} = m_{pl}$ [see expressions (D3) and (D5)]. This property guarantees the existence of real solutions of the eigenproblem (12).

APPENDIX E: HIGH-ENERGY ASYMPTOTICS

We present and compare the asymptotic high-energy behavior of the quasiclassical Green's function in the diffusive limit within the Usadel approximation to the more general case described by the Eilenberger equation. Since the present discussion is independent of the presence or absence of a weak exchange field $J \ll \epsilon_f$ in the system, we leave it out.

1. Diffusive limit

The Usadel equation[46] for arbitrary temperatures (not necessarily close to T_c as in the rest of the paper) is

$$[i\varepsilon_n \hat{\tau}_3 - \hat{\Delta}, \hat{g}] + \frac{D}{\pi} \partial_x (\hat{g} \partial_x \hat{g}) = \hat{0}, \quad \text{(E1)}$$

where $\hat{g}$ is a 4×4 matrix in combined particle-hole and spin spaces, $\hat{\tau}_j$ ($j = 1, 2, 3$) are the Pauli matrices in particle-hole space, and $\hat{\Delta}$ is the gap function [$\hat{\Delta} = (i\sigma_y)\hat{\tau}_1 \Delta$ if Δ is real]. Equation (E1) is supplemented with a normalization condition

$$\hat{g}^2 = -\pi^2 \hat{1}. \quad \text{(E2)}$$

Further details concerning the structure of the Green's function with the present notation can be found in Ref. 43 (see also Ref. 55).

At high energies the order parameter and the derivative term are small,

$$\Delta \sim T_{c0} \ll \varepsilon_n, \quad \text{(E3)}$$

$$D/\xi^2 \sim T_{c0} \ll \varepsilon_n, \quad \text{(E4)}$$

and we expand the Green's function

$$\hat{g} = \hat{g}^{(0)} + \hat{g}^{(1)} + \hat{g}^{(2)} + \cdots, \quad \text{(E5)}$$

where the term $\hat{g}^{(k)}$ is of order $(T_{c0}/\varepsilon_n)^k$. To lowest order we have

$$[i\varepsilon_n \hat{\tau}_3, \hat{g}^{(0)}] = 0, \quad \text{(E6)}$$

$$(\hat{g}^{(0)})^2 = -\pi^2 \hat{1}, \quad \text{(E7)}$$

with the solution

$$\hat{g}^{(0)} = (-i\pi)\,\mathrm{sgn}(\varepsilon_n)\hat{\tau}_3. \quad \text{(E8)}$$

In first order we obtain

$$[i\varepsilon_n \hat{\tau}_3, \hat{g}^{(1)}] = [\hat{\Delta}, \hat{g}^{(0)}], \quad \text{(E9)}$$

$$\hat{g}^{(0)}\hat{g}^{(1)} + \hat{g}^{(1)}\hat{g}^{(0)} = 0. \tag{E10}$$

Since $\hat{g}^{(0)}$ is proportional to $\hat{\tau}_3$, the second line can be used to move $\hat{g}^{(1)}$ to one side of the commutator on the left-hand side of the first line. We obtain

$$2i\varepsilon_n\hat{\tau}_3\hat{g}^{(1)} = [\hat{\Delta}, \hat{g}^{(0)}]. \tag{E11}$$

The solution is purely off-diagonal in particle-hole space

$$\hat{g}^{(1)} = \frac{(-i\pi)}{2i|\varepsilon_n|}(\hat{\tau}_3\hat{\Delta}\hat{\tau}_3 - \hat{\Delta}) = \frac{\pi}{|\varepsilon_n|}\hat{\Delta}. \tag{E12}$$

In second order we have

$$[i\varepsilon_n\hat{\tau}_3, \hat{g}^{(2)}] = -\frac{D}{\pi}\hat{g}^{(0)}\partial_x^2\hat{g}^{(1)}, \tag{E13}$$

$$\hat{g}^{(0)}\hat{g}^{(2)} + \hat{g}^{(2)}\hat{g}^{(0)} + (\hat{g}^{(1)})^2 = 0. \tag{E14}$$

After a short calculation, similar to the calculation in first order, we obtain

$$\hat{g}^{(2)} = \frac{(-i\pi)}{2\varepsilon_n|\varepsilon_n|}\hat{\tau}_3\hat{\Delta}^2 + \frac{\pi D}{2\varepsilon_n^2}\partial_x^2\hat{\Delta}. \tag{E15}$$

Note, in particular, that there is an off-diagonal term proportional to $1/\varepsilon_n^2$ for inhomogeneous systems.

The off-diagonal part of the Green's function has according to the above the asymptotic form

$$f(\varepsilon_n, x) = \frac{\pi\Delta(x)}{|\varepsilon_n|} + \frac{\pi D\partial_x^2\Delta(x)}{2\varepsilon_n^2} + \mathcal{O}\left[\left(\frac{T_{c0}}{|\varepsilon_n|}\right)^3\right], \tag{E16}$$

which we now use to discuss the gap equation. The gap equation

$$\Delta(x) = \lambda T \sum_{|\varepsilon_n|<\omega_p} f(\varepsilon_n, x), \tag{E17}$$

contains a log-divergence and it is necessary to introduce a cutoff ω_p. But by the well-known procedure (see, e.g., Ref. 56), the interaction strength λ and the Matsubara sum cutoff ω_p can both be eliminated by adding and subtracting the leading high-energy term in Eq. (E16). The gap equation then has the form in Eq. (5). The Matsubara sum converges, with a high-energy asymptotic tail $\propto 1/\varepsilon_n^2$ according to Eq. (E16), and can be extended to infinity. In practice, a technical cutoff ε_c is introduced that should, however, be high enough that the results of the calculation are cutoff independent.

2. Arbitrary mean free path

We compare the above results obtained within the Usadel approximation with the corresponding high-energy behavior obtained within the Eilenberger approach. The Eilenberger equation[57,58] reads

$$[i\varepsilon_n\hat{\tau}_3 - \hat{\Delta} - \hat{\sigma}_{\text{imp}}, \hat{g}] + i\vec{v}_f\cdot\nabla\hat{g} = \hat{0}, \tag{E18}$$

with impurity self energy $\hat{\sigma}_{\text{imp}}$, and where $\vec{v}_f$ is the Fermi velocity. The normalization condition $\hat{g}^2 = -\pi^2\hat{1}$ holds. We include nonmagnetic impurity scattering within the self-consistent t-matrix approximation, for which the impurity self-energy is

$$\hat{\sigma}_{\text{imp}}(s) = c\hat{t}(s,s), \tag{E19}$$

where c is the impurity concentration, and s is a parameter that specifies the position of the momentum on the Fermi surface. The t matrix is given as the solution of the equation

$$\hat{t}(s,s') = \hat{u}(s,s') + \langle\hat{u}(s,s'')\mathcal{N}_f(s'')\hat{g}(s'')\hat{t}(s'',s')\rangle_{s''}, \tag{E20}$$

where we have omitted for brevity all variables except the Fermi momentum. Here, $\hat{u}(s,s') = u(s,s')\hat{1}$ is the impurity scattering potential, and $\langle\cdots\rangle_{s'}$ denotes a Fermi surface average over s'.

We expand $\hat{g}$ as in Eq. (E5). The zeroth-order term for the Green function is given analogously to the discussion for the diffusive limit by

$$\hat{g}^{(0)} = (-i\pi)\text{sgn}(\varepsilon_n)\hat{\tau}_3. \tag{E21}$$

For the higher orders we need to expand the impurity t matrix in the parameter (T_{c0}/ε_n),

$$\hat{t} = \hat{t}^{(0)} + \hat{t}^{(1)} + \hat{t}^{(2)} + \cdots, \tag{E22}$$

and similarly for the impurity self-energy. Introducing the operator

$$\hat{D}(s,s') = \delta(s-s')\hat{1} - u(s,s')\mathcal{N}_f(s')\hat{g}^{(0)}, \tag{E23}$$

the t-matrix equation for the zeroth-order term $\hat{t}^{(0)}$ takes the form

$$\langle\hat{D}(s,s'')\hat{t}^{(0)}(s'',s')\rangle_{s''} = \hat{u}(s,s'). \tag{E24}$$

With the inverse operator $\hat{D}^{-1}$ defined by

$$\langle\hat{D}^{-1}(s,s'')\hat{D}(s'',s')\rangle_{s''} = \delta(s-s')\hat{1}, \tag{E25}$$

the formal solutions are given by

$$\hat{t}^{(0)}(s,s') = \langle\hat{D}^{-1}(s,s'')\hat{u}(s'',s')\rangle_{s''},$$

$$\hat{t}^{(1)}(s,s') = \langle\hat{t}^{(0)}(s,s'')\mathcal{N}_f(s'')\hat{g}^{(1)}(s'')\hat{t}^{(0)}(s'',s')\rangle_{s''}. \tag{E26}$$

From Eq. (E26) we obtain

$$[\hat{\sigma}_{\text{imp}}^{(0)}, \hat{g}^{(0)}] = \hat{0}, \tag{E27}$$

as a result of $[\hat{u}, \hat{\tau}_3] = \hat{0}$. Consequently, the first-order term for $\hat{g}$ is, in complete analogy to the discussion leading to Eq. (E12), given by

$$\hat{g}^{(1)} = \frac{\pi}{|\varepsilon_n|}\hat{\Delta}. \tag{E28}$$

Finally, for the second-order term $\hat{g}^{(2)}$, we have

$$[i\varepsilon_n\hat{\tau}_3,\hat{g}^{(2)}]=[\hat{\sigma}^{(1)}_{\rm imp},\hat{g}^{(0)}]+[\hat{\sigma}^{(0)}_{\rm imp},\hat{g}^{(1)}]-i\vec{v}_f\cdot\nabla\hat{g}^{(1)}. \tag{E29}$$

We solve this equation by using the normalization condition, Eq. (E14). Restricting ourselves to isotropic impurity scattering, we obtain[59]

$$\hat{g}^{(2)}=\frac{(-i\pi)}{2\varepsilon_n|\varepsilon_n|}\hat{\tau}_3\left(i\vec{v}_f\cdot\nabla\hat{\Delta}-\hat{\Delta}^2+\frac{i\,\mathrm{sgn}(\varepsilon_n)}{\tau}\hat{\tau}_3\{\hat{\Delta}-\langle\hat{\Delta}\rangle_s\}\right), \tag{E30}$$

where the inverse scattering time is defined as

$$\frac{1}{\tau}=2\pi c\mathcal{N}_f\frac{u^2}{1+\pi^2\mathcal{N}_f^2u^2}. \tag{E31}$$

For an isotropic (s-wave) superconducting order parameter the last term in Eq. (E30) vanishes. In this case, the second-order high-energy contribution from Eq. (E30) is odd in frequency, and it drops out of the Matsubara sum. The leading order contribution comes in third order[59] and the high-energy tail of the Matsubara sum is $\propto 1/|\varepsilon_n|^3$. This means that the technical cutoff ε_c can be chosen much smaller than in the diffusive limit within the Usadel approximation.

The different high-energy asymptotics within the Eilenberger and Usadel approaches are due to the diffusive approximation employed by Usadel: the impurity self-energy, i.e., the inverse scattering time $1/\tau$, is at the outset assumed to be the largest energy scale in the problem. The high-energy tail is different depending on the order in which the limits $\tau\to 0$ and $\varepsilon_c\to\infty$ are taken.

APPENDIX F: ANALYTIC SUMMATION OF THE HIGH-ENERGY TAIL IN THE FOURIER SERIES APPROACH

At high energies $\varepsilon_n\gg T_{c0}$ and J, the matrix $\hat{W}$ has a simple energy dependence that we exploit to sum the Matsubara sum to infinity. That is, we write

$$m_{lp}=\bar{m}_{lp}+\mathcal{R}_{lp}, \tag{F1}$$

where $\bar{m}_{lp}$ includes terms in the sum in Eqs. (D3) and (D4) up to a technical cutoff ε_c while the rest term $\mathcal{R}_{lp}$ is the sum from ε_c to infinity computed analytically below.

At high energies $W_{12}=-W_{21}\approx 0$, while

$$W_{11}\approx\frac{\gamma_1}{1+\gamma_{b1}\lambda}, \tag{F2}$$

$$W_{22}\approx-\frac{\gamma_2}{1+\gamma_{b2}\lambda}, \tag{F3}$$

where $\lambda^2=\varepsilon_n/\pi T_{c0}$. These relations hold for both the trilayer and the pentalayer, which reflects the fact that the theory becomes local at high energies [see the effective boundary condition (6)]. The key function of the Fourier method then has the form

$$b_{lp}=\frac{\xi_s}{d_s}\frac{2}{\lambda}\frac{c_1+c_2\lambda}{c_3+c_4\lambda+c_5\lambda^2}, \tag{F4}$$

where

$$c_1=\gamma_1+(-1)^{l+p}\gamma_2+\gamma_1\gamma_2[1+(-1)^{l+p}], \tag{F5}$$

$$c_2=\gamma_1\gamma_{b2}+(-1)^{l+p}\gamma_2\gamma_{b1}, \tag{F6}$$

$$c_3=1+\gamma_1+\gamma_2+\gamma_1\gamma_2, \tag{F7}$$

$$c_4=\gamma_1\gamma_{b2}+\gamma_2\gamma_{b1}+\gamma_{b1}+\gamma_{b2}, \tag{F8}$$

$$c_5=\gamma_{b1}\gamma_{b2}. \tag{F9}$$

For each element of the matrix m_{lp} we can perform the high-energy Matsubara sum by integration. We get

$$\mathcal{R}_{lp}=\delta_{lp}\frac{1}{\pi}\ln\left(1+\frac{p^2}{\tilde{d}_s^2}\frac{T_{c0}}{\varepsilon_c}\right)+\frac{2}{\pi^2}\frac{1}{\tilde{d}_s}I_{lp},$$

$$I_{lp}=\int_{\varepsilon_c/T_{c0}}^{\infty}\frac{c_1\sqrt{x}+c_2x}{\left(x+\frac{l^2}{\tilde{d}_s^2}\right)\left(x+\frac{p^2}{\tilde{d}_s^2}\right)(c_3+c_4\sqrt{x}+c_5x)}dx, \tag{F10}$$

where we used the short-hand notation $\tilde{d}_s=d_s/\pi\xi_s$. Note that Eq. (F10) is independent of the temperature T and only depends on the parameters in Eqs. (F5)–(F9), on d_s, and on the cutoff ε_c.

[1] A. I. Buzdin and M. Yu. Kupriyanov, JETP Lett. **52**, 487 (1990).
[2] Z. Radovic, M. Ledvij, L. Dobrosavljevic-Grujic, A. I. Buzdin, and J. R. Clem, Phys. Rev. B **44**, 759 (1991).
[3] A. I. Buzdin, B. Bujicic, and M. Yu. Kupriyanov, Sov. Phys. JETP **74**, 124 (1992).
[4] E. A. Demler, G. B. Arnold, and M. R. Beasley, Phys. Rev. B **55**, 15174 (1997).
[5] L. R. Tagirov, Phys. Rev. Lett. **83**, 2058 (1999).
[6] A. I. Buzdin, A. V. Vedyayev, and N. V. Ryzhanova, Europhys. Lett. **48**, 686 (1999).
[7] I. Baladié, A. Buzdin, N. Ryzhanova, and A. Vedyayev, Phys. Rev. B **63**, 054518 (2001).
[8] Ya. V. Fominov, N. M. Chtchelkatchev, and A. A. Golubov, JETP Lett. **74**, 96 (2001); Phys. Rev. B **66**, 014507 (2002).
[9] I. Baladié and A. Buzdin, Phys. Rev. B **67**, 014523 (2003).
[10] Y. V. Fominov, A. A. Golubov, and M. Y. Kupriyanov, JETP Lett. **77**, 510 (2003).
[11] C.-Y. You, Ya. B. Bazaliy, J. Y. Gu, S.-J. Oh, L. M. Litvak, and S. D. Bader, Phys. Rev. B **70**, 014505 (2004).
[12] J. S. Jiang, D. Davidović, D. H. Reich, and C. L. Chien, Phys.

Rev. Lett. **74**, 314 (1995).
[13] Th. Mühge, N. N. Garif'yanov, Yu. V. Goryunov, G. G. Khaliullin, L. R. Tagirov, K. Westerholt, I. A. Garifullin, and H. Zabel, Phys. Rev. Lett. **77**, 1857 (1996).
[14] J. Aarts, J. M. E. Geers, E. Brück, A. A. Golubov, and R. Coehoorn, Phys. Rev. B **56**, 2779 (1997).
[15] L. Lazar, K. Westerholt, H. Zabel, L. R. Tagirov, Yu. V. Goryunov, N. N. Garif'yanov, and I. A. Garifullin, Phys. Rev. B **61**, 3711 (2000).
[16] J. Y. Gu, C.-Y. You, J. S. Jiang, J. Pearson, Ya. B. Bazaliy, and S. D. Bader, Phys. Rev. Lett. **89**, 267001 (2002).
[17] A. Yu. Rusanov, M. Hesselberth, J. Aarts, and A. I. Buzdin, Phys. Rev. Lett. **93**, 057002 (2004).
[18] Y. Obi, M. Ikebe, and H. Fujishiro, Phys. Rev. Lett. **94**, 057008 (2005).
[19] C. Cirillo, S. L. Prischepa, M. Salvato, C. Attanasio, M. Hesselberth, and J. Aarts, Phys. Rev. B **72**, 144511 (2005).
[20] A. Potenza and C. H. Marrows, Phys. Rev. B **71**, 180503(R) (2005).
[21] I. C. Moraru, W. P. Pratt, and N. O. Birge, Phys. Rev. Lett. **96**, 037004 (2006).
[22] A. Yu. Rusanov, S. Habraken, and J. Aarts, Phys. Rev. B **73**, 060505(R) (2006).
[23] D. Stamopoulos and M. Pissas, Phys. Rev. B **73**, 132502 (2006).
[24] A. I. Buzdin, Rev. Mod. Phys. **77**, 935 (2005).
[25] A. I. Buzdin, L. N. Bulaevskii, and S. V. Panyukov, JETP Lett. **35**, 178 (1982).
[26] V. V. Ryazanov, V. A. Oboznov, A. Yu. Rusanov, A. V. Veretennikov, A. A. Golubov, and J. Aarts, Phys. Rev. Lett. **86**, 2427 (2001).
[27] H. Sellier, C. Baraduc, F. Lefloch, and R. Calemczuk, Phys. Rev. Lett. **92**, 257005 (2004).
[28] S. M. Frolov, D. J. Van Harlingen, V. A. Oboznov, V. V. Bolginov, and V. V. Ryazanov, Phys. Rev. B **70**, 144505 (2004).
[29] T. Kontos, M. Aprili, J. Lesueur, F. Genêt, B. Stephanidis, and R. Boursier, Phys. Rev. Lett. **89**, 137007 (2002).
[30] Y. Blum, A. Tsukernik, M. Karpovski, and A. Palevski, Phys. Rev. Lett. **89**, 187004 (2002).
[31] W. Guichard, M. Aprili, O. Bourgeois, T. Kontos, J. Lesueur, and P. Gandit, Phys. Rev. Lett. **90**, 167001 (2003).
[32] V. Shelukhin, A. Tsukernik, M. Karpovski, Y. Blum, K. B. Efetov, A. F. Volkov, T. Champel, M. Eschrig, T. Löfwander, G. Schön, and A. Palevski, Phys. Rev. B **73**, 174506 (2006).
[33] F. S. Bergeret, A. F. Volkov, and K. B. Efetov, Phys. Rev. Lett. **86**, 3140 (2001).
[34] A. A. Golubov, M. Yu. Kupriyanov, and Ya. V. Fominov, JETP Lett. **75**, 190 (2002).
[35] Ya. M. Blanter and F. W. J. Hekking, Phys. Rev. B **69**, 024525 (2004).
[36] F. S. Bergeret, A. F. Volkov, and K. B. Efetov, Phys. Rev. B **64**, 134506 (2001).
[37] F. S. Bergeret, A. F. Volkov, and K. B. Efetov, Phys. Rev. B **68**, 064513 (2003).
[38] F. S. Bergeret, A. F. Volkov, and K. B. Efetov, Phys. Rev. Lett. **86**, 4096 (2001).
[39] A. F. Volkov, F. S. Bergeret, and K. B. Efetov, Phys. Rev. Lett. **90**, 117006 (2003).
[40] A. Kadigrobov, R. I. Shekhter, and M. Jonson, Europhys. Lett. **54**, 394 (2001); Low Temp. Phys. **27**, 760 (2001).
[41] M. Eschrig, J. Kopu, J. C. Cuevas, and G. Schön, Phys. Rev. Lett. **90**, 137003 (2003).
[42] T. Champel and M. Eschrig, Phys. Rev. B **71**, 220506(R) (2005).
[43] T. Champel and M. Eschrig, Phys. Rev. B **72**, 054523 (2005).
[44] T. Löfwander, T. Champel, J. Durst, and M. Eschrig, Phys. Rev. Lett. **95**, 187003 (2005).
[45] F. S. Bergeret, A. F. Volkov, and K. B. Efetov, Rev. Mod. Phys. **77**, 1321 (2005).
[46] K. D. Usadel, Phys. Rev. Lett. **25**, 507 (1970).
[47] F. S. Bergeret, A. F. Volkov, and K. B. Efetov, Phys. Rev. B **65**, 134505 (2002).
[48] A. Bagrets, C. Lacroix, and A. Vedyayev, Phys. Rev. B **68**, 054532 (2003).
[49] M. Yu. Kupriyanov and V. F. Lukichev, Sov. Phys. JETP **67**, 1163 (1988).
[50] P. Fulde and R. A. Ferrell, Phys. Rev. **135**, A550 (1964).
[51] A. J. Larkin and Y. N. Ovchinnikov, Zh. Eksp. Teor. Fiz. **47**, 1136 (1964) [Sov. Phys. JETP **20**, 762 (1965)].
[52] A. B. Vorontsov and J. A. Sauls, Phys. Rev. B **68**, 064508 (2003).
[53] A. B. Vorontsov and J. A. Sauls, cond-mat/0601565.
[54] S. Tollis, J. Cayssol, and A. Buzdin, Phys. Rev. B **73**, 174519 (2006).
[55] J. A. X. Alexander, T. P. Orlando, D. Rainer, and P. M. Tedrow, Phys. Rev. B **31**, 5811 (1985).
[56] D. Xu, S.-K. Yip, and J. A. Sauls, Phys. Rev. B **51**, 16233 (1995).
[57] G. Eilenberger, Z. Phys. **214**, 195 (1968).
[58] A. I. Larkin and Y. N. Ovchinnikov, Zh. Eksp. Teor. Fiz. **55**, 2262 (1968) [Sov. Phys. JETP **28**, 1200 (1969)].
[59] M. Eschrig, Ph.D. thesis, Bayreuth University (1997).